Check for updates

ADVANCING EARTH AND SPACE SCIENCE

JGR Atmospheres

RESEARCH ARTICLE
10.1029/2019JD032172

Key Points:
- A new mathematical method for solving SCE is first proposed and developed
- This method shows excellent agreement with the Sectional Method which is used as reference
- The new method is verified as an efficient and reliable numerical scheme for studying atmospheric aerosol dynamics

Correspondence to:
M. Yu,
yumz@ieecas.cn

Citation:
Shen, J., Yu, M., Chan, T. L., Tu, C., & Liu, Y. (2020). Efficient method of moments for simulating atmospheric aerosol growth: Model description, verification, and application. *Journal of Geophysical Research: Atmospheres*, *125*, e2019JD032172. https://doi.org/10.1029/2019JD032172

Received 2 DEC 2019
Accepted 7 MAY 2020
Accepted article online 15 MAY 2020

Author Contributions:
Conceptualization: M. Yu
Data curation: C. Tu, Y. Liu
Methodology: J. Shen
Supervision: T. L. Chan
Validation: M. Yu
Writing - original draft: M. Yu, Y. Liu
Writing – review & editing: M. Yu, T. L. Chan

©2020. American Geophysical Union. All Rights Reserved.

Efficient Method of Moments for Simulating Atmospheric Aerosol Growth: Model Description, Verification, and Application

J. Shen[1], M. Yu[1], T. L. Chan[2], C. Tu[1], and Y. Liu[1]

[1]Laboratory of Aerosol Science and Technology, China Jiliang University, Hangzhou, China, [2]Department of Mechanical Engineering, The Hong Kong Polytechnic University, Kowloon, Hong Kong

Abstract The atmospheric aerosol dynamics model (AADM) has been widely used in both comprehensive air quality model systems and chemical transport modeling globally. The AADM consists of Smoluchowski's coagulation equation (SCE), whose solution undergoing Brownian coagulation in the free molecular regime is a challenge because it is inconsistent with aerosols whose size distribution cannot exactly follow the lognormal size distribution. Thus, a new method for solving the SCE without assuming lognormal size distribution is proposed and developed. The underlying principle of this method is that the hybridization of the well-established method of moments with the assumed lognormal size distribution (log MOM) and Taylor-series expansion method of moments (TEMOM) is implemented. This method shows excellent agreement with the sectional method (SM) which is used as reference. The accuracy of these two specific models closely approaches that of the TEMOM, but overcomes the limitation of the classical log MOM. The computational time of this scheme is considerably lower than that of the SM. The new method was successfully implemented to reveal the formation and growth of secondary particles emitted from a vehicle exhaust tailpipe. It was found that the formation of new particles only occurs in the interface region of the turbulent exhaust jet (which is very close to the tailpipe exit), whereas no new particles are formed in the mixture of the exhaust jet plume and the surrounding cold air downstream. The new method is verified as an efficient and reliable numerical scheme for studying atmospheric aerosol dynamics.

1. Introduction

The contribution of aerosols to both climate change (Rosenfeld, 2006; Rosenfeld et al., 2014, 2019) and air pollution (Huang et al., 2014; Kumar et al., 2014; Wang et al., 2019; Yao et al., 2018; Yuan et al., 2019) has received increased recognition. Correspondingly, aerosol dynamics models have been included in both global chemistry and transport simulations and regional air quality simulations for over half a century (Gama et al., 2019; Hass et al., 2003; Herzog et al., 2004; Jasor et al., 2005; Karydis et al., 2007; Lauer et al., 2005; Sportisse, 2007; Vignati et al., 2004; Whitby & McMurry, 1997; Zhou et al., 2016). In all developed aerosol dynamics models, aerosol dynamics—which dominate the evolution of particle size distribution—are managed separately to meet the requirement of numerical simulation. These aerosol dynamics processes usually include nucleation, coagulation, condensation-evaporation, and deposition. Brownian coagulation is an important mechanism that leads to instability of aerosols and has attracted more interest from scientists compared with other aerosol dynamics because of its mathematical complexity. The end result of coagulation is a continuous decrease in particle number concentration and an increase in particle size. The theory for illustrating this phenomenon was originally introduced based on Smoluchowski's equation and then followed by Muller's development (Müller, 1928; Petitti et al., 2013). Muller's equation is expressed as

$$\frac{\partial n(v,\,t)}{\partial t} = \frac{1}{2}\int_0^v \beta(v_1, v - v_1)n(v_1, t)n(v - v_1, t)\mathrm{d}v_1 - n(v,\,t)\int_0^\infty \beta(v_1, v)n(v_1, t)\mathrm{d}v_1, \tag{1}$$

where particle volume, v, is used rather than particle diameter because the volumes are additive. The first term on the right-hand side of Equation 1 is the rate of formation of particles of size v by smaller particles of sizes v_1 and $v - v_1$. The factor 1/2 is introduced because collisions are counted twice in the

integral. The second term of Equation 1 accounts for the loss of particles of size v by collisions with all other particles. Equation 1 was known as Smoluchowski's coagulation equation (SCE), which was further developed in the aerosol community to include other aerosol dynamics processes including nucleation, condensation-evaporation, and deposition, and also to couple with climate models by considering air convection and diffusion. The developed Equation 1 is now recognized as the particle general dynamics equation (PGDE), which is the key equation of all weather and air pollution forecast codes, including the Weather Research and Forecasting model coupled to Chemistry (WRF-Chem), the University of Helsinki Multicomponent Aerosol model, and the European Air Pollution Dispersion modeling system (EURAD; Ackermann et al., 1998; Grabowski et al., 2019; Korhonen et al., 2004; Kukkonen et al., 2012).

In theory, almost all important aerosol quantities, which determine the property of aerosols as well as its direct or indirect effects on air pollution and climate, such as number concentration, mass concentration, and size distribution of particles, can be obtained by solving the PGDE numerically (Wright et al., 2001). The PGDE is usually solved by numerical methods. There have been some important achievements, including the development of the sectional method (SM; Bruns & Ezekoye, 2012; Gelbard et al., 1980; Kostoglou, 2007; Landgrebe & Pratsinis, 1990), method of moments (MOM; Fox et al., 2008; Liu, Chan, Lin, et al., 2019; McGraw, 1997; Petitti et al., 2013; Pratsinis, 1988; Rani et al., 2014; Tang & Lin, 2013; Yu et al., 2008), Monte Carlo method (Kraft, 2005; Morgan et al., 2006), and stochastic particle method (Debry et al., 2003; Kruis et al., 2012; Menz et al., 2014; Rani et al., 2014; Sabelfeld, 1998). These four different types of numerical methods have been widely applied in weather and air pollution forecast codes. Among these, the MOM is usually regarded as the most economical and is also the most suitable for coupling with an air transport equation, such as the Navier-Stokes equations (McGraw et al., 2008; Passalacqua et al., 2018; Yu & Lin, 2018). It should be noted that the MOM with predefined lognormal size distribution is still the classic method used in the most common weather and air pollution forecast codes, such as the WRF-Chem and EURAD (Cai et al., 2016; Gama et al., 2019). Furthermore, the SM is also used for modeling aerosol dynamics in nuclear reactor safety applications (Herranz et al., 2018).

The key to the MOM is to implement a transformation from particle size distribution (PSD) function space, $\{n(v)\}$ in Equation 1, to the space of moments, $\{m_k\}$. When transferring from $\{n(v)\}$ to $\{m_k\}$, the closure problem for ordinary differential equations (ODEs) appears, which needs to be resolved using closure schemes. There have been several schemes to achieve closure, which can be divided into two categories, namely quadrature-based MOM (QBMOM) and nonquadrature-based MOM (NBMOM). The predefined particle size distributed method, pth-order polynomial MOM, MOM with interpolative closure, and Taylor-series expansion MOM (TEMOM) all belong to the NBMOM. An advantage of the NBMOM is that the transferred moment ODEs can be written as their explicit form (Yu & Lin, 2018). It should be noted that the QBMOM, especially the Gaussian quadrature MOM (QMOM and direct QMOM [DQMOM]; Marchisio & Fox, 2005; Robert McGraw, 1997) has been the most widely used MOM to couple with computational fluid dynamics until very recently. Among all NBMOMs, the predefined lognormal MOM was the first to be proposed for solving the PGDE (Cohen & Vaughan, 1971), and it now governs the establishment of atmospheric aerosol models, including the WRF-Chem and EURAD. When implementing the lognormal MOM by transferring from the PSD function space, $\{n(v)\}$, to the space of moments, $\{m_k\}$, the collision kernel must be written as an equivalent linear expression for $v^p v_1^q$ (p and q are arbitrary real numbers). This requirement limits the application of log MOM because some kernels cannot easily be obtained with an equivalent linear expression for $v^p v_1^q$. Although the QBMOM is currently the most widely used of the MOMs owing to contributions from the research teams of Fox (Heylmun et al., 2019; Kong & Fox, 2017; Marchisio & Fox, 2005; Vikas et al., 2013) and McGraw (McGraw, 1997; McGraw et al., 2008), the NBMOM, such as the log MOM and TEMOM, still has wide applications. This is because such methods have high numerical efficiency and do not require the calculation of eigen systems and have no ill-conditioned matric problems.

Brownian coagulation in the free molecular regime is a key mechanism affecting the evolution of aerosol size distribution with particle Knudsen number ($\mathrm{Kn} = \frac{\lambda}{r}$, where λ is the mean free path of air, and r is the particle radius) larger than 10 (Friedlander, 2000). The collision kernel in this regime includes a term $(1/v + 1/v_1)^{1/2}$, which is a major obstacle for expressing the kernel by an equivalent linear expression, as it does

21698996, 2020, 13, Downloaded from https://agupubs.onlinelibrary.wiley.com/doi/10.1029/2019JD032172 by Hong Kong Poly University, Wiley Online Library on [16/05/2024]. See the Terms and Conditions (https://onlinelibrary.wiley.com/terms-and-conditions) on Wiley Online Library for rules of use; OA articles are governed by the applicable Creative Commons License

for the transfer of SCE to the moment ODEs. Some effort has been made to overcome this technical difficulty. The most successful outcome is the strategy proposed by Lee et al. (1984), in which the factor $(1/v+1/v_1)^{1/2}$ is substituted by $b[(1/v)^{1/2}+(1/v_1)^{1/2}]$; the SCE can then be transferred to moment ODEs with both implicit and explicit moments. In order to achieve the final closure of moment ODEs, Equation 11 is needed. Unfortunately, the value of b is an unmanageable issue in Equation 9, which has to be obtained by solving integral equations with varying initial PSDs. Pratsinis (1988) further developed and expressed the term, b, as a function of geometric standard deviation of PSD. However, both the studies by Lee et al. (1984) and Pratsinis (1988) have the limitation that the expression of the value b has to be determined numerically in advance, which inevitably leads to uncertainty in mathematics. Hence, a highly efficient and precise method becomes essential to approximate this collision kernel.

The TEMOM was proposed by Yu et al. (2008) to solve SCE. The key to the TEMOM is to approximate any expressions using their truncated Taylor expansion series with adjusted errors; thus, the technical difficulty in the log MOM might be overcome by the TEMOM. Whether the TEMOM and log MOM can be hybridized for the solution of SCE remains an open question.

In this study, a new method to explicitly solve the SCE undergoing Brownian coagulation in the free molecular regime is presented. The underlying principle of this method is that the approximations of collision kernel and explicit moments are achieved by the hybridization of the well-established log MOM and TEMOM. In order to distinguish from other methods of moments, the new approach is referred to as "hybrid-TEMOM-Log MOM." The new method is also different from some promising analytical or semianalytical methods for solving the SCE (Anand & Mayya, 2011; Turco & Yu, 1997). Since there are two different hybrid processes involved, the terms hybrid TEMOM-log MOM (I) and hybrid TEMOM-log MOM (II) are used to distinguish them. The SM as a reference is used to validate this new scheme of hybrid TEMOM-log MOM, which is regarded as an exact solution of SCE by the Aerosol Society (Otto et al., 1999) as well as our previous work (Yu et al., 2016; Yu & Lin, 2017a). In addition, the results from both TEMOM and log MOM are presented for comparative studies. The moment ODEs obtained from the proposed scheme have explicit expressions and are thus more easily programed than the well-established log MOM. The proposed hybrid TEMOM-log MOM (I) is further utilized to study the formation and growth of secondary particles emitted from a vehicle exhaust tailpipe, in which an advanced parameterized model for binary homogeneous nucleation of sulfuric acid-water vapors is introduced. The competing processes of binary nucleation, condensation, and coagulation are clearly revealed.

The paper is organized as follows. In section 2, a model description of the hybrid TEMOM-log MOM method is presented, and the numerical errors are fully analyzed. In section 3, the numerical details of studied cases are provided and all the governing equations are dealt with using a normalized method. In section 4, the results and discussion are presented for comparisons among the new hybrid TEMOM-log MOM, TEMOM, log MOM, and SM, and the validation of the new method is carried out. In this section, the new scheme is further utilized to study the exhaust particles emitted from the vehicle tailpipe. The factors affecting secondary nanoparticle formation and subsequent growth in a turbulent jet exhaust plume are revealed.

2. Materials and Methods

In the present study, Brownian coagulation in the free molecular regime is considered because it is the most difficult to deal with using the MOM (Pratsinis, 1988). For the studied case, the coagulation kernel is given by (Friedlander, 2000):

$$\beta(v,v_1) = B_1(1/v+1/v_1)^{1/2}\left(v^{1/3}+v_1{}^{1/3}\right)^2, \tag{2}$$

where $B_1 = (3/4\pi)^{1/6}(6k_BT/\rho_p)^{1/2}$, k_B is the Boltzmann constant, T is the gas temperature, and ρ_p is the mass density of the particles.

To implement the MOM, the system of Equation 1 is transferred to a system of moment ODEs with respect to the moment. The moment transformation involves multiplying Equation 1 by v and then integrating it over the entire particle size distribution to obtain the moment-transformed equations of the PSD (Lee et al., 1984):

21698996, 2020, 13, Downloaded from https://agupubs.onlinelibrary.wiley.com/doi/10.1029/2019JD032172 by Hong Kong Poly University, Wiley Online Library on [16/05/2024]. See the Terms and Conditions (https://onlinelibrary.wiley.com/terms-and-conditions) on Wiley Online Library for rules of use; OA articles are governed by the applicable Creative Commons License

$$\frac{\mathrm{d}m_k}{\mathrm{d}t} = \frac{1}{2}\int_0^\infty \int_0^\infty \kappa(v, v_1, k) n(v,\ t) n(v_1, t) \mathrm{d}v \mathrm{d}v_1, \tag{3}$$

where $\kappa(v, v_1, k) = [(v+v_1)^k - v^k - {v_1}^k]\ \beta(v, v_1)$. The moment m_k is defined by

$$m_k = \int_0^\infty v^k n(v) \mathrm{d}v. \tag{4}$$

The dynamic behavior of an aerosol can be described from the rate of change of its first three moments (Pratsinis, 1988). According to the present study on the log MOM and TEMOM, only the first three moments are considered here,

$$\kappa(v, v_1, k) = \left[(v+v_1)^k - v^k - {v_1}^k\right]\beta(v, v_1) \qquad = \begin{cases} -\beta(v, v_1), & k{=}0, \\ 0, & k{=}1, \\ 2vv_1\beta(v, v_1), & k{=}2. \end{cases} \tag{5}$$

2.1. Two Technical Difficulties in the MOM

If only $k = 0$, 1, and 2 are involved, Equation 3 can be written as follows:

$$\begin{cases} \dfrac{\mathrm{d}m_0}{\mathrm{d}t} = -\dfrac{1}{2}\displaystyle\int_0^\infty \int_0^\infty \beta(v, v_1) n(v,\ t) n(v_1, t) \mathrm{d}v \mathrm{d}v_1, \\ \dfrac{\mathrm{d}m_1}{\mathrm{d}t} = 0, \\ \dfrac{\mathrm{d}m_2}{\mathrm{d}t} = \displaystyle\int_0^\infty \int_0^\infty vv_1\beta(v, v_1) n(v,\ t) n(v_1, t) \mathrm{d}v \mathrm{d}v_1. \end{cases} \tag{6}$$

The purpose of the MOM is to remove an integral operator on the right-hand sides of Equation 6. Unfortunately, two essential technical difficulties arise from the PSD function space, $\{n(v)\}$, to the space of moments, $\{m_k\}$, that is, the binary polynomial approximation and the closure function for any order moment.

2.1.1. Binary Polynomial Approximation

To introduce Equation 4 into Equation 6, the collision kernel, $\beta(v, v_1)$, must be expressed as a binary additive form, that is,

$$\widetilde{\beta}(v, v_1) = \sum_{p\ \in\ R} \sum_{q\ \in\ R} a_{pq} v^p {v_1}^q \approx \beta(v, v_1), \tag{7}$$

where p and q are arbitrary real numbers and a_{pq} is the coefficient. Unfortunately, the presence of the term $(1/v + 1/v_1)^{1/2}$ in Equation 2 makes the binary additive form unavailable.

2.1.2. Closure Function

Even if Equation 7 is available and the terms on the right-hand sides of Equation 6 can be expressed as functions of moments, these moments are usually not explicit, which results in the nonclosure of transferred moment ODEs. A general closure function that can be used to replace any kth moments becomes necessary. In Equation 6, only the first three moments, namely m_0, m_1, and m_2, are explicit, and thus the general closure function can be expressed as

$$m_k = f_{\text{closure}}(m_0, m_1, m_2), \tag{8}$$

where k is an arbitrary real number.

It should be noted that both log MOM and TEMOM have the same aforementioned problems, and the corresponding solutions to them are given by direct and explicit formulations as Equations 7 and 8.

21698996, 2020, 13, Downloaded from https://agupubs.onlinelibrary.wiley.com/doi/10.1029/2019JD032172 by Hong Kong Poly University, Wiley Online Library on [16/05/2024]. See the Terms and Conditions (https://onlinelibrary.wiley.com/terms-and-conditions) on Wiley Online Library for rules of use; OA articles are governed by the applicable Creative Commons License

2.2. Two Polynomial Approximations to the Kernel in the Free Molecule Regime

2.2.1. Lognormal Kernel (Log-Kernel)

In previous work by Lee et al. (1984), the term $(1/v + 1/v_1)^{1/2}$ is approximated as

$$\left(\frac{1}{v}+\frac{1}{v_1}\right)^{\frac{1}{2}} \approx b\left(\frac{1}{v^{\frac{1}{2}}}+\frac{1}{v_1^{\frac{1}{2}}}\right), \tag{9}$$

where

$$b = \int_0^\infty\int_0^\infty v^k\beta(v,v_1)n(v,\ t)n(v_1,t)\mathrm{d}v\mathrm{d}v_1 \times \left\{\int_0^\infty\int_0^\infty \left[\frac{\left(\frac{1}{v^{1/2}}+\frac{1}{v_1^{1/2}}\right)}{(v+v_1)^{1/2}}\right]\times v^k\beta(v,v_1)n(v,t)n(v_1,t)\mathrm{d}v\mathrm{d}v_1\right\}^{-1}. \tag{10}$$

To obtain the coefficient b in Equation 10, the numerical calculation must be carried out. In addition, b is a value dependent on the initial geometric standard deviation, σ_0 in the work of Lee et al. (1984) and Pratsinis (1988). It implies that b has different values for different PSD. This defines the approach to dealing with the uncertainty of $(1/v + 1/v_1)^{1/2}$ in mathematics. Although Pratsinis (1988) tried to write b as a function of σ_0, the relative errors of the real values of such an approach cannot be obtained. Furthermore, for calculating the value of b, many hypotheses and simplifications have to be involved, including the assumption of time-dependent lognormal size distribution. It led to the motivation to develop a more reliable way to deal with the approximation of $(1/v + 1/v_1)^{1/2}$ in the present study.The collision kernel in the free molecular regime, that is, Equation 2, can be further expressed if the log MOM is implemented as follows,

$$\beta(v,v_1) = Kb_k\left(v^{\frac{2}{3}}v_1^{-\frac{1}{2}} + 2v^{\frac{1}{3}}v_1^{-\frac{1}{6}} + v_1^{\frac{1}{6}} + v^{\frac{1}{6}} + 2v^{-\frac{1}{6}}v_1^{\frac{1}{3}} + v^{-\frac{1}{2}}v_1^{\frac{2}{3}}\right) \triangleq \widetilde{\beta}_{\mathrm{Log}}(v,v_1). \tag{11}$$

Here, the approximating kernel $\widetilde{\beta}_{\mathrm{Log}}(v,v_1)$ is called a lognormal kernel (Log-kernel).

2.2.2. Binary Taylor Expansion Kernel (Taylor-Kernel)

In the TEMOM, the term $(1/v + 1/v_1)^{1/2}$ is approximated with a binary additive form by implementing a binary Taylor-series expansion technique (Yu et al., 2008) Without loss of generality, $f(v,v_1) = (v + v_1)^{1/2}$ can then be defined as

$$\begin{aligned} f(v,v_1) = {} & f(u,\ u) + \left[(v-u)\frac{\partial}{\partial v} + (v_1-u)\frac{\partial}{\partial v_1}\right]f(u,\ u) + \frac{1}{2!}\left[(v-u)\frac{\partial}{\partial v} + (v_1-u)\frac{\partial}{\partial v_1}\right]^2 f(u,\ u) + \cdots \\ & + \frac{1}{n!}\left[(v-u)\frac{\partial}{\partial v} + (v_1-u)\frac{\partial}{\partial v_1}\right]^n f(u,\ u) \\ & + \frac{1}{(n+1)!}\left[(v-u)\frac{\partial}{\partial v} + (v_1-u)\frac{\partial}{\partial v_1}\right]^{n+1} f(u+\theta(v-u),\ u+\theta(v_1-u)),\ (0<\theta<1). \end{aligned} \tag{12}$$

here, the $[u,u]$ are binary Taylor-series expansion points, which can be defined as $u = m_1/m_0$. The error R_n is denoted as

$$R_n = \frac{1}{(n+1)!}\left[(v-u)\frac{\partial}{\partial v} + (v_1-u)\frac{\partial}{\partial v_1}\right]^{n+1} f(u+\theta(v-u),\ u+\theta(v_1-u)), \tag{13}$$

and the absolute error$|R_n|$ is denoted as

$$|R_n| \le \frac{M}{(n+1)!}(|v-u|+|v_1-u|)^{n+1} = \frac{M}{(n+1)!}\rho^{n+1}(|\cos\alpha|+|\sin\alpha|)^{n+1} \le \frac{(\sqrt{2})^{n+1}}{(n+1)!}M\rho^{n+1}, \tag{14}$$

where M is a positive number and $\rho = \sqrt{(v-u)^2 + (v_1-u)^2}$. $\cos\alpha = \frac{v-u}{\rho}$, $\sin\alpha = \frac{v_1-u}{\rho}$. When $\rho \to 0$, that is, $v \to u$ and $v_1 \to u$ simultaneously, the absolute error $|R_n| \to 0$ and the rate of convergence is $O(\rho^{n+1})$. It implies that the binary additive form in Equation 12 is theoretically reasonable when the volume of

21698996, 2020, 13, Downloaded from https://agupubs.onlinelibrary.wiley.com/doi/10.1029/2019JD032172 by Hong Kong Poly University, Wiley Online Library on [16/05/2024]. See the Terms and Conditions (https://onlinelibrary.wiley.com/terms-and-conditions) on Wiley Online Library for rules of use; OA articles are governed by the applicable Creative Commons License

aerosol particles approaches the average value. If the Taylor series expansion point is u, the term $(1/v + 1/v_1)^{1/2}$ is approximated by the following expression,

$$(v+v_1)^{1/2} \approx \frac{3\sqrt{2u}}{8} + \frac{3\sqrt{2}v}{8\sqrt{u}} + \frac{3\sqrt{2}v_1}{8\sqrt{u}} - \frac{\sqrt{2}v^2}{32u^{3/2}} - \frac{\sqrt{2}vv_1}{16u^{3/2}} - \frac{\sqrt{2}{v_1}^2}{32u^{3/2}}. \tag{15}$$

Then, the collision kernel in the free molecule regime can now be approximated as follows:

$$\beta(v, v') = B_1(\varphi_1\phi_1 + \varphi_2\phi_2 + \varphi_3\phi_3) \triangleq \widetilde{\beta}_{\text{Taylor}}(v, v_1) \tag{16}$$

where

$$\varphi_1 = v^{\frac{1}{6}}v_1^{-\frac{1}{2}} + 2v^{-\frac{1}{6}}v_1^{-\frac{1}{6}} + v_1^{\frac{1}{6}}v^{-\frac{1}{2}}$$

$$\varphi_2 = v^{\frac{7}{6}}v_1^{-\frac{1}{2}} + v^{-\frac{1}{2}}v_1^{\frac{7}{6}} + 2v^{\frac{5}{6}}v_1^{-\frac{1}{6}} + 2v_1^{\frac{5}{6}}v^{-\frac{1}{6}} + v^{\frac{1}{2}}v_1^{\frac{1}{6}} + v^{\frac{1}{6}}v_1^{\frac{1}{2}}$$

$$\varphi_3 = 4v^{\frac{5}{6}}v_1^{\frac{5}{6}} + 2v^{\frac{7}{6}}v_1^{\frac{1}{2}} + 2v^{\frac{1}{2}}v_1^{\frac{7}{6}} + v^{\frac{3}{2}}v_1^{\frac{1}{6}} + v^{\frac{1}{6}}v_1^{\frac{3}{2}} + v^{\frac{13}{6}}v_1^{-\frac{1}{2}} + v^{-\frac{1}{2}}v_1^{\frac{13}{6}} + 2v^{\frac{11}{6}}v_1^{-\frac{1}{6}} + 2v^{-\frac{1}{6}}v_1^{\frac{11}{6}}$$

$$\phi_1 = \frac{3\sqrt{2}}{8}{u_0}^{1/2}$$

$$\phi_2 = \frac{3\sqrt{2}}{8}{u_0}^{-1/2}$$

$$\phi_3 = -\frac{\sqrt{2}}{32}{u_0}^{-3/2}$$

In the implement of TEMOM, φ_1, φ_2, and φ_3 can be simplified to be the following expression given the symmetric in v, v_1 (Yu et al., 2017),

$$\varphi_1 = 2v^{1/6}v'^{-1/2} + 2v^{-1/6}v'^{-1/6}$$

$$\varphi_2 = 2v^{7/6}v'^{-1/2} + 4v^{5/6}v'^{-1/6} + 2v^{1/2}v'^{1/6}$$

$$\varphi_3 = 4v^{\frac{5}{6}}v'^{\frac{5}{6}} + 4v^{\frac{7}{6}}v'^{\frac{1}{2}} + 2v^{\frac{3}{2}}v'^{\frac{1}{6}} + 2v^{\frac{13}{6}}v'^{-\frac{1}{2}} + 4v^{\frac{11}{6}}v'^{-\frac{1}{6}}$$

Here, the approximating kernel $\widetilde{\beta}_{\text{Taylor}}(v, v_1)$ is called the binary Taylor expansion kernel (Taylor-kernel).

Substituting the log-kernel into Equation 11 and the Taylor-kernel in Equation 16 into the moment ODEs of Equation 5 results in the following systems, respectively,

$$\begin{cases} \dfrac{\mathrm{d}m_0}{\mathrm{d}t} = -\dfrac{1}{2}\int_0^\infty\int_0^\infty \widetilde{\beta}_{\text{Log}}(v, v_1)n(v, t)n(v_1, t)\mathrm{d}v\mathrm{d}v_1 \\ \dfrac{\mathrm{d}m_1}{\mathrm{d}t} = 0 \\ \dfrac{\mathrm{d}m_2}{\mathrm{d}t} = \int_0^\infty\int_0^\infty vv_1\widetilde{\beta}_{\text{Log}}(v, v_1)n(v, t)n(v_1, t)\mathrm{d}v\mathrm{d}v_1 \end{cases}. \tag{17}$$

and

$$\begin{cases} \dfrac{\mathrm{d}m_0}{\mathrm{d}t} = -\dfrac{1}{2}\int_0^\infty\int_0^\infty \widetilde{\beta}_{\text{Taylor}}(v, v_1)n(v, t)n(v_1, t)\mathrm{d}v\mathrm{d}v_1 \\ \dfrac{\mathrm{d}m_1}{\mathrm{d}t} = 0 \\ \dfrac{\mathrm{d}m_2}{\mathrm{d}t} = \int_0^\infty\int_0^\infty vv_1\widetilde{\beta}_{\text{Taylor}}(v, v_1)n(v, t)n(v_1, t)\mathrm{d}v\mathrm{d}v_1. \end{cases} \tag{18}$$

2.3. Two Closure Functions in the MOM

Both log MOM and TEMOM are widely considered to be promising methods for solving SCE with very few computational costs. As discussed in section 2.1, both Equations 17 and 18 need to be further closed using suitable closure functions. In the log MOM, the closure function is obtained based on an assumption of

21698996, 2020, 13, Downloaded from https://agupubs.onlinelibrary.wiley.com/doi/10.1029/2019JD032172 by Hong Kong Poly University, Wiley Online Library on [16/05/2024]. See the Terms and Conditions (https://onlinelibrary.wiley.com/terms-and-conditions) on Wiley Online Library for rules of use; OA articles are governed by the applicable Creative Commons License

time-dependent lognormal size distribution, whereas in the TEMOM the closure function is obtained by expanding v^k within a manageable error. If the log MOM closure function (Lee et al., 1984) is applied to Equation 17 and the TEMOM closure function (Yu et al., 2008) is applied to Equation 18, the new schemes are presented as that found below.

2.3.1. Hybrid TEMOM-Log MOM (I)

In the TEMOM, the closure function has the following expression:

$$m_k = \left(\frac{u^{k-2}k^2}{2} - \frac{u^{k-2}k}{2}\right)m_2 + \left(-u^{k-1}k^2 + 2u^{k-1}k\right)m_1 + \left(u^k + \frac{u^k k^2}{2} - \frac{3u^k k}{2}\right)m_0 \quad \triangleq m_{k_{\text{Taylor}}}, \left(u = \frac{m_1}{m_0}\right). \tag{19}$$

As Equation 19 is applied to Equation 17, a new scheme of hybrid TEMOM-log MOM (I) is derived:

$$\begin{cases} \dfrac{\mathrm{d}m_0}{\mathrm{d}t} = B_1 b \dfrac{m_0^{11/6}\left(41m_0^2m_2^2 - 190m_0m_1^2m_2 - 2443m_1^4\right)}{648m_1^{23/6}} \\ \dfrac{\mathrm{d}m_1}{\mathrm{d}t} = 0 \\ \dfrac{\mathrm{d}m_2}{\mathrm{d}t} = -B_1 b \dfrac{65m_0^2m_2^2 - 670m_0m_1^2m_2 - 1987m_1^4}{324m_0^{\frac{1}{6}}m_2^{\frac{11}{6}}}. \end{cases} \tag{20}$$

It should be noted here that Equation 19 can be replaced with its developed version shown for acquiring more accurate approximated accuracy (Yu et al., 2015).

2.3.2. Hybrid TEMOM-Log MOM (II)

In the log MOM, the closure function is obtained by assuming the lognormal PSD (Lee et al., 1984),

$$m_k = m_0^{1-\frac{3}{2}k+\frac{1}{2}k^2} m_1^{2k-k^2} m_2^{-\frac{1}{2}k+\frac{1}{2}k^2}. \tag{21}$$

The derivation of Equation 21 is shown in section A.3. As Equation 21 is applied to Equation 18, another new scheme of hybrid TEMOM-log MOM (II) for solving SCE can be expressed as:

$$\begin{cases} \dfrac{dm_0}{dt} = -\dfrac{B_1\sqrt{2}m_0^{\frac{59}{36}}m_1^{\frac{5}{9}}}{16m_2^{\frac{7}{36}}}\left(-g^{\frac{11}{6}} + 12g^{\frac{2}{3}} + 11g^{\frac{1}{2}} + 12g^{\frac{7}{18}} + 24g^{\frac{2}{9}} - 2g^{\frac{1}{6}} - 2g^{\frac{19}{18}} - 2g^{\frac{1}{18}} + 12\right) \\ \dfrac{dm_1}{dt} = 0 \\ \dfrac{dm_2}{dt} = -\dfrac{B_1\sqrt{2}m_1^{\frac{22}{9}}}{8m_0^{\frac{11}{36}}m_2^{\frac{5}{36}}}\left(g^{\frac{31}{9}} - 24g^{\frac{5}{6}} - 12g^{\frac{23}{18}} + 2g^{\frac{16}{9}} + 2g^{\frac{8}{3}} + 2g^{\frac{5}{3}} + g^{\frac{19}{9}} - 12g^{\frac{1}{9}} - 12g^{\frac{11}{18}} - 12\right) \end{cases} \tag{22}$$

where, $g = \dfrac{m_0m_2}{m_1^2}$. To be noted here, the same as the log MOM, the hybrid TEMOM-log MOM (II) can be only applied to aerosols with lognormal size distribution because of its closure function shown in Equation 21, while the hybrid TEMOM-log MOM (I) has no such limitation.

2.4. Family of TEMOM-Log MOM

According to the aforementioned schemes, four MOM models can be classified for solving SCE by adjusting the combination of the binary polynomial kernels and the closure functions, which constitutes a family of TEMOM-log MOM as shown in Figure 1.

Both the log MOM and TEMOM have been verified as reliable methods for solving SCE. However, the newly proposed and developed hybrid TEMOM-log MOM (I) and (II) have never been verified before. Equations 20 and 22 have explicit expressions; thus, the numerical algorithms can be written using a very simple approach. In the well-established log MOM widely used in the atmospheric aerosol dynamics model (Pratsinis, 1988); however, the ODEs have to be closed using a lognormal size distributed assumption.

21698996, 2020, 13, Downloaded from https://agupubs.onlinelibrary.wiley.com/doi/10.1029/2019JD032172 by Hong Kong Poly University, Wiley Online Library on [16/05/2024]. See the Terms and Conditions (https://onlinelibrary.wiley.com/terms-and-conditions) on Wiley Online Library for rules of use; OA articles are governed by the applicable Creative Commons License

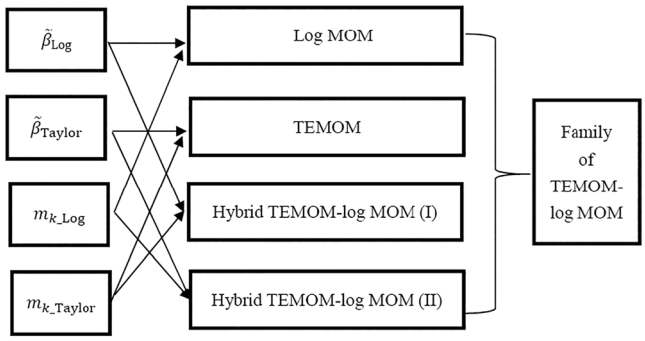

Figure 1. Spanning map of the family of TEMOM-log MOM.

3. Computational Description

The SM is selected as a reference and is implemented under the same condition as the hybrid TEMOM-log MOM (I) and (II) models. The relative errors of the hybrid TEMOM-log MOM (I) and (II) models to the SM are discussed in section 4. In the present study, the SM model is mainly used for validating MOMs and is solved using the same computer code as that used in (Yu & Lin, 2017b). The log MOM and TEMOM are also implemented for comparison purposes. The solution with the assumption of an initial lognormal PSD is used (Barrett & Jheeta, 1996). Hence, the kth moment can be represented by

$$m_k = M_k\left(N_0 v_{g_0}^k\right), \tag{23}$$

where v_{g_0} is the initial geometric mean volume. When the normalized terms are implemented in the moment ODEs, as shown in Equations 20 and 23, N_0 and v_{g_0} are included in the normalized time. Under this condition, the dimensionless time with respect to the coagulation kernel in the free molecular regime is

$$\tau = B_1 N_0 v_{g_0}^{1/6} t. \tag{24}$$

When Equation 25 is introduced into Equations 20 and 22, the normalized equations for the hybrid models (I) and (II) are obtained, as presented in section A.4. The initial moments can be expressed as

$$M_{k0} = \chi^{k^2}, \tag{25}$$

where $\chi = e^{\left(3\ln\sigma_{g0}\right)^2/2}$. The normalization using Equations 23–25 are applied in sections 4.1 and 4.3. To be consistent with that used in Yu et al. (2009), $N_0 = 5.0 \times 10^{19}$ #/m^3 and $d_{g0} = 0.4 \times 10^{-9}$ m. The parameter d_{g0} is selected for the diameter of the H_2SO_4 molecule. It should be noted here that the selection of both N_0 and d_{g0} is only to implement the normalization of both Equations 20 and 23; it does not mean that the model validation is implemented relying on H_2SO_4 molecular coagulation.

4. Results and Discussion

Both the numerical precision and efficiency of the newly proposed method for solving SCE are evaluated to verify its reliability in sections 4.1 and 4.2. In section 4.3, the application of the newly proposed method to the study of the formation and growth of secondary particles in a turbulent exhaust jet plume is discussed.

4.1. Model Validation

The purpose of this section is to verify the numerical precision of the newly proposed and developed hybrid (I) and (II) models. To achieve this, the hybrid models (I) and (II), log MOM, TEMOM, and SM are applied to solve the same SCE under the same conditions. Four crucial moments, namely M_0, $M_{1/3}$, $M_{2/3}$, and M_2, are evaluated. The relative errors of the kth moments of the investigated methods of moments to the SM are expressed as follows:

$$RE = \frac{M_k(\text{MOM}) - M_k(\text{SM})}{M_k(\text{SM})}, \tag{26}$$

where M_k (MOM) is the kth moments obtained from the investigated MOM and M_k (SM) is the corresponding moments obtained from the referenced SM. All numerical calculations are implemented using the fourth-order Runge-Kutta method with a fixed time step of 0.001. The SM, log MOM, and TEMOM were verified in Park et al. (1999), Yu et al. (2008, 2015), and Yu and Lin (2017b).

Figure 2 provides a comparison of the variances of four essential moments with respect to time among these two new hybrid models, log MOM (Lee et al., 1984), and TEMOM (Yu et al., 2008). In the numerical calculation, the initial geometric standard deviation of particle number distribution, $\sigma_{g0} = 1.2$. The zeroth moment,

21698996, 2020, 13, Downloaded from https://agupubs.onlinelibrary.wiley.com/doi/10.1029/2019JD032172 by Hong Kong Poly University, Wiley Online Library on [16/05/2024]. See the Terms and Conditions (https://onlinelibrary.wiley.com/terms-and-conditions) on Wiley Online Library for rules of use; OA articles are governed by the applicable Creative Commons License

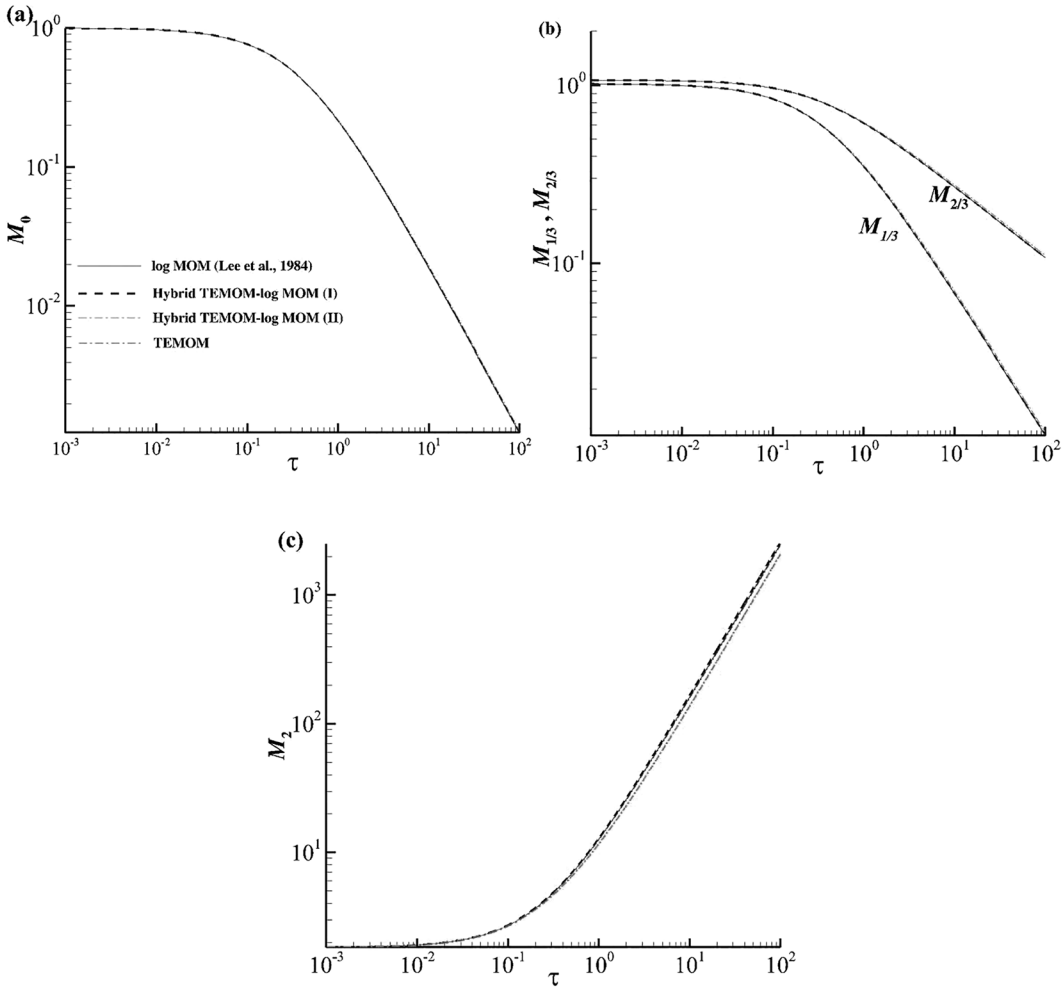

Figure 2. Variance of kth moments ((a) M_0, (b) $M_{1/3}$ and $M_{2/3}$, and (c) M_2) with time produced by the family of TEMOM-log MOM.

M_0, represents the particle number concentration; the 1/3th moment, $M_{1/3}$, is a quantity characterizing particle diameter; The 2/3th moment, $M_{2/3}$, is a quantity characterizing particle surface area concentration. The 2nd moment (M_2) have no actual physical meanings, but it is an essential part to get other important physical quantities of aerosols such as geometric standard deviation of particle number distribution is given in Equation 27. For three investigated moments, namely M_0, $M_{1/3}$, and $M_{2/3}$, all curves overlap with each other, while for M_2 only the hybrid TEMOM-log MOM (II) deviates slightly from the other three models. The comparison implies that the hybrid TEMOM-log MOM (I), log MOM, and TEMOM have almost the same numerical precision for solving SCE undergoing Brownian coagulation in the free molecular regime. The hybrid TEMOM-log MOM (II) has only a slight difference compared with the other three models.

For a better evaluation of the reliability of the new method, the relative errors (REs) of the four moments of the TEMOM-log MOM family to the referenced SM were investigated, as shown in Figure 3. The SM is usually considered as an exact numerical solution to the SCE (Otto et al., 1999). It is clear that these four methods in the TEMOM-log MOM family have almost the same variance trend and the maximum relative error of the hybrid TEMOM-log MOM (II) found in M_0, $M_{1/3}$, $M_{2/3}$, and M_2, respectively. In addition, the other three methods almost overlap with each other, especially for $M_{2/3}$. The REs of these four methods almost overlap with each other again as $\tau \rightarrow 10^2$ for M_0, $M_{2/3}$, and M_2, respectively. It is therefore concluded that the newly proposed and developed hybrid models, especially TEMOM-log MOM (I), have nearly the same numerical accuracy as the TEMOM and log MOM. Compared with the models of TEMOM-log MOM (I) and (II), the TEMOM-log MOM (I) has higher numerical accuracy.

21698996, 2020, 13, Downloaded from https://agupubs.onlinelibrary.wiley.com/doi/10.1029/2019JD032172 by Hong Kong Poly University, Wiley Online Library on [16/05/2024]. See the Terms and Conditions (https://onlinelibrary.wiley.com/terms-and-conditions) on Wiley Online Library for rules of use; OA articles are governed by the applicable Creative Commons License

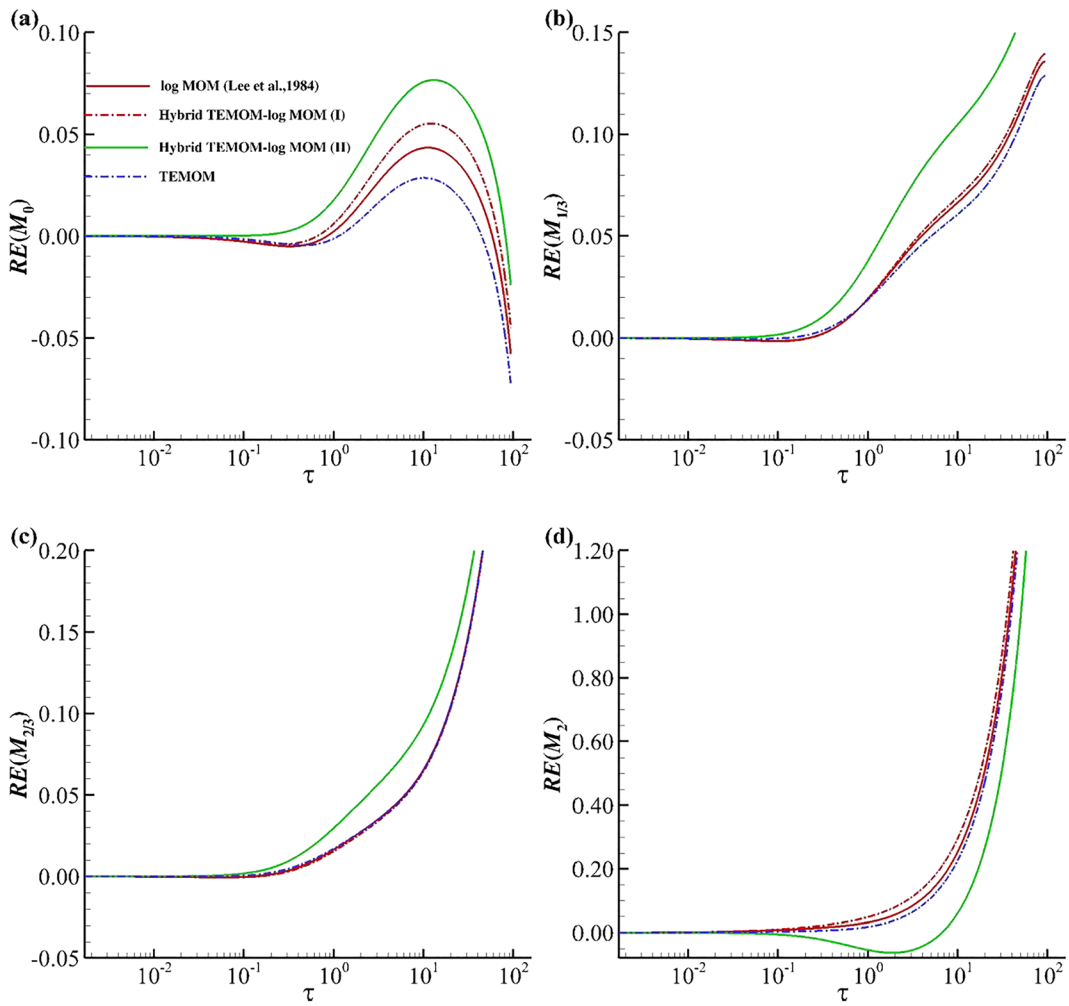

Figure 3. Relative errors of kth moments ((a) M_0, (b) $M_{1/3}$, (c) $M_{2/3}$, and (d) M_2) of the TEMOM-log MOM family to the referenced SM in the free molecular regime.

The geometric standard deviation, σ_g, of the particle number distribution is a crucial indicator for characterizing the properties of PSD. The log MOM has the capability to directly produce the value of σ_g according to the first three moments (Lee et al., 1984). The other MOMs, such as QMOM and TEMOM, were verified to have the same capability of producing σ_g, using the same moments as the log MOM (Yu et al., 2008). Thus, σ_g can be used as an indicator to verify the investigated methods. If an aerosol can be assumed to have a lognormal PSD, σ_g can be expressed as a function of the first three moments (Pratsinis, 1988):

$$\ln^2\sigma_g = \frac{1}{9}\ln\left(\frac{M_0 M_2}{M_1^2}\right). \tag{27}$$

In Figure 4, the values of σ_g for various investigated methods are presented and compared. The values of σ_g from all MOMs of the TEMOM-log MOM family achieve their own asymptotic values. The asymptotic value of σ_g of TEMOM is 1.345, which is the closest to the value produced by the QMOM with six nodes (1.346; Yu et al., 2008). As expected, both the hybrid TEMOM-log MOM (I) and (II) models achieve their asymptotic values. The values of σ_g of the log MOM and the hybrid TEMOM-log MOM (I) and (II) models are 1.355, 1.365, and 1.315, respectively (Yu et al., 2008). The hybrid TEMOM-log MOM (I) model generates nearly the same σ_g as the TEMOM and log MOM, whereas the hybrid TEMOM-log MOM (II) model deviates from the other three investigated methods. By evaluating the four moments and their geometric standard deviations, it is concluded that the hybrid TEMOM-log MOM (I) model is a more precise method

21698996, 2020, 13, Downloaded from https://agupubs.onlinelibrary.wiley.com/doi/10.1029/2019JD032172 by Hong Kong Poly University, Wiley Online Library on [16/05/2024]. See the Terms and Conditions (https://onlinelibrary.wiley.com/terms-and-conditions) on Wiley Online Library for rules of use; OA articles are governed by the applicable Creative Commons License

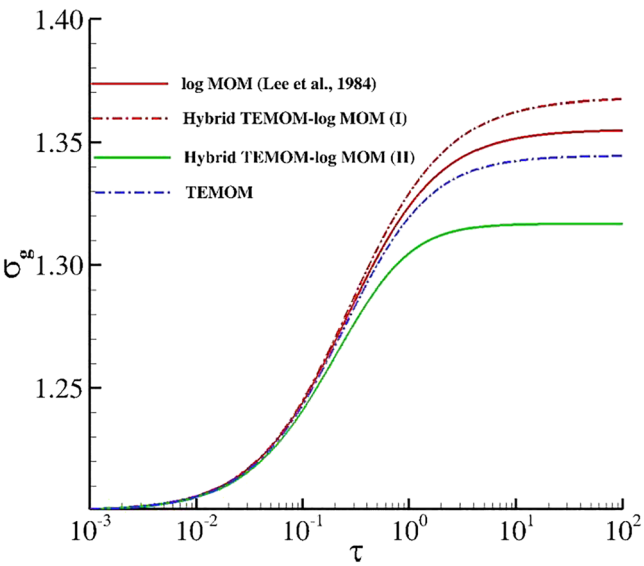

Figure 4. Geometric standard deviations of the particle number distributions derived from the family of TEMOM-log MOM.

than the hybrid TEMOM-log MOM (II). The TEMOM-log MOM (I) model has very nearly the same numerical precision as the TEMOM and log MOM in numerical precision.

4.2. Numerical Efficiency

Numerical precision and efficiency are equally important to determine the feasibility of any numerical models. Here, all four investigated moment models, as well as the SM, are implemented to $\tau = 100$. The numerical efficiency of investigated models is also evaluated by comparing their computational times. For the SM, the section number is 500, which ensures the high numerical accuracy of this SM method.

Table 1 shows the computational time consumed by different investigated models. The ODEs are all solved numerically by executing the fourth-order Runge-Kutta method with a fixed time step, 0.001, using an Intel(R) Core (TM) i7-3,820 CPU and Microsoft Visual Studio. The 0.001 time step is selected because the numerical accuracy under the same time step was validated in our previous study (Yu et al., 2008). Relative to all the MOMs, the SM consumes a relatively very large computational time. The consumed time of the TEMOM-log MOM (I) model is almost the same as TEMOM, but is smaller than the log MOM and TEMOM-log MOM (II) models. Comparing Equation 22 with 20 reveals that the mathematical form of the TEMOM-log MOM (II) is much more complex than that of the TEMOM-log MOM (I); thus, the former requires more numerical calculations at each time step. Therefore, it is concluded that the numerical efficiency of the TEMOM-log MOM (I) model is clearly greater than the SM, log MOM, and TEMOM-log MOM (II) models and is even greater than the well-known TEMOM. It should be noted that SM has unavoidable advantage to give the detailed size distribution and to estimate the fraction of particles exceeding a given size (Anand et al., 2012), which is not possible by MOMs.

In conclusion, the TEMOM-log MOM (I) model was found to be a promising model for solving SCE, in terms of both numerical efficiency and accuracy. In addition, this model has wider applications than the current log MOM because it overcomes the shortcoming of the log MOM with the prerequirement of assumed lognormal PSD. In the following section, the TEMOM-log MOM (I) model is utilized to study the secondary nanoparticle formation and subsequent growth in a turbulent jet plume.

4.3. Application of TEMOM-Log MOM (I) Model

It has been determined that in the atmospheric environment, most nanoparticles come from a multicomponent route, that is, a binary homogeneous nucleation process of water-sulfuric acid vapors. A complete theoretical understanding of this phenomenon is still a challenge due to its complicated chemical/physical processes (Chan, Liu, & Chan, 2010; Chan, Zhou, et al., 2010; Harrison et al., 2018; Liu & Chan, 2018; Maurya et al., 2018; Nagpure et al., 2011; Olin et al., 2019; Zhou & Chan, 2011). Because of the undoubted contribution of gaseous and particulate emissions to air pollution emitted from power plants and motor vehicles into the atmosphere (Chan, Liu, & Chan, 2010; Chan, Zhou, et al., 2010; Chan & Ning, 2005; Ning et al., 2005; Wang et al., 2006; Zhou & Chan, 2011), a lot of attention has been focused on secondary particles. Most particles emitted by engines are in the nanoparticle range (i.e., d_p<50 nm), especially with the improvement of advanced engine technologies and after-treatment devices. More and more evidence suggests that nanoparticles have a more negative effect on human health than particles of micrometers or larger (Gnach et al., 2015; Harrison et al., 2018). This has raised the important question of how to control the emission of nanoparticles before and after emission conditions. Hence, it is essential to have a better understanding of the dynamic processes of nanoparticle formation and subsequent growth in the atmospheric environment.

Table 1
Computational Time Taken to Execute the Fourth-Order Runge-Kutta Method With a Fixed Time Step, 0.001

Method	Computational time	Predefined PSD
SM	~72.00 hr	No
TEMOM	~5.05 s	No
Log MOM	~6.00 s	Yes
TEMOM-log MOM (I)	~5.00 s	No
TEMOM-log MOM (II)	~8.08 s	Yes

21698996, 2020, 13, Downloaded from https://agupubs.onlinelibrary.wiley.com/doi/10.1029/2019JD032172 by Hong Kong Poly University, Wiley Online Library on [16/05/2024]. See the Terms and Conditions (https://onlinelibrary.wiley.com/terms-and-conditions) on Wiley Online Library for rules of use; OA articles are governed by the applicable Creative Commons License

The evolution of secondary particles in exhausts is a complicated physical–chemical process, which involves momentum, heat and mass transfer, binary homogeneous nucleation, Brownian coagulation, Brownian and turbulent diffusions, condensation, and thermophoresis (Liu, Chan, & Liu, 2019). To determine this, the appropriate numerical model is coupled with the Navier-Stokes equations for flows and the general dynamic equation for particles. One-way coupling is implemented since nanoparticles have very little effect on the surrounding continuum. It should be noted that only secondary particle formation and growth emitted from a tailpipe exist is concerned.

4.3.1. Governing Equations

4.3.1.1. Governing Equations for Fluid Flow

Nanoparticles have a very small Stokes number in fluid flows, which suggests that particles can follow the fluid without disturbing it. In the present study, the Navier-Stokes equations for incompressible flows are

$$\frac{\partial u_i}{\partial x_i} = 0, \tag{28a}$$

$$\frac{\partial u_i}{\partial t} + u_j \frac{\partial u_i}{\partial x_j} = -\frac{1}{\rho}\frac{\partial p}{\partial x_i} + \frac{\partial}{\partial x_j}\left(\nu \frac{\partial u_i}{\partial x_j}\right), \tag{28b}$$

$$\frac{\partial \rho h}{\partial t} + \frac{\partial \rho h u_j}{\partial x_j} = \frac{\partial}{\partial x_j}\left(\frac{k_t}{C_p}\frac{\partial h}{\partial x_j}\right), \tag{28c}$$

where u_i is the velocity, p is the filtered pressure, h is the specific enthalpy, k_t is the thermal conductivity, and $C_p$is the specific heat at a constant pressure. The indexes i, j are taken as 1, 2 and refers to the x and y directions, respectively. The $k - \varepsilon$ turbulent model scheme is utilized to solve Equations 28a–28c regarding the effect of turbulence on the flow.

4.3.1.2. Governing Equations for Particles

Within the Smoluchowski mean-field theory, the particle number concentration, $n(v,t)$, is represented as a function in terms of particle volume, v, and time, t. Taking into consideration the physical terms of fluid convection, thermophoretic drift, Brownian and turbulent diffusion, Brownian coagulation, condensation, and nucleation, the governing equation for $n(v,t)$ can be expressed as

$$\begin{aligned}\frac{\partial n(v,\{x_i\},t)}{\partial t} &+ \underbrace{\frac{\partial\left(u_j n(v,\{x_j\},t)\right)}{\partial x_j}}_{\text{convection}} + \underbrace{\frac{\partial\left((u_{th})_j n(v,\{x_j\},t)\right)}{\partial x_j}}_{\text{thermophoresis}} = \underbrace{\frac{\partial}{\partial x_j}\left(\Gamma \frac{\partial n(v,\{x_j\},t)}{\partial x_j}\right)}_{\text{diffusion}} \\ &+ \underbrace{\frac{1}{2}\int_{v^*}^{v}\beta(v-v',v')n(v-v',\{x_i\},t)n(v',\{x_i\},t)\mathrm{d}v' - n(v,\{x_i\},t)\int_{v^*}^{\infty}\beta(v,v')n(v',\{x_i\},t)\mathrm{d}v'}_{\text{coagulation}} \\ &+ \underbrace{\frac{\partial G n(v,\{x_i\},t)}{\partial v}}_{\text{condensation}} + \underbrace{J(v^*,\{x_i\},t)\delta(v-v^*)}_{\text{nucleation}},\end{aligned} \tag{29}$$

where Γ is the sum of the turbulent diffusion and Brownian diffusion coefficients ($\Gamma = \Gamma_t + \Gamma_B$), $\beta(v,v')$ is the coagulation kernel between particles of two volumes as shown in Equation 2, J is the nucleation rate, v^* is the volume of a stable sulfuric acid-water (H_2SO_4-H_2O) monomer, δ is the Kronecker Delta function, and u_{th} is the thermophoretic velocity. G is the growth rate of the nucleus volume due to condensation. In atmospheric environment, the growth rate due to condensation process can be obtained by first finding out impinging rate of H_2SO_4 molecules onto to the particle and then calculating the H_2SO_4 content in the aerosol using the generalized Kelvin equation for binary mixtures. Under the condition, the particle growth rate takes the following form (Van Dingenen & Raes, 1991)

$$G = \left.\frac{\mathrm{d}v}{\mathrm{d}t}\right|_{SA} \times \frac{x v_{\mathrm{a}} + (1-x)v_{\mathrm{w}}}{x v_{\mathrm{a}}}\ , \tag{30}$$

where $\left.\frac{\mathrm{d}v}{\mathrm{d}t}\right|_{SA} = \frac{\pi {d_{\mathrm{p}}}^2 v_{\mathrm{a}}(p_1 - p_{\mathrm{d}})}{(2\pi m k_{\mathrm{b}} T)^2}$ in the free molecular regime, d_{p} is the diameter of existing particle, m is the mass of H_2SO_4 molecular, p_1 is the partial pressure of H_2SO_4 vapor in the gas, v_{a} is the volume of a H_2SO_4 molecule, p_{d} is the partial pressure of H_2SO_4 vapor at the particle surface given by the Kelvin equation,

21698996, 2020, 13, Downloaded from https://agupubs.onlinelibrary.wiley.com/doi/10.1029/2019JD032172 by Hong Kong Poly University, Wiley Online Library on [16/05/2024]. See the Terms and Conditions (https://onlinelibrary.wiley.com/terms-and-conditions) on Wiley Online Library for rules of use; OA articles are governed by the applicable Creative Commons License

v_w is the volume of water molecule, and the mole fraction of sulfuric acid, x, is taken from Kelvin equation.

Equation 29 is usually called the general dynamics equation (GDE), which cannot be directly coupled with Equations 28a–28c for calculation because it has too many degrees relative to the particle volume v. In order to overcome the shortcoming of the GDE, a suitable numerical scheme is to transfer Equation 29 with respect to $\{n(v,t)\}$ to the moment $\{m_k\}$. The moment transformation involves multiplying Equation 29 by v and then integrating it over the entire PSD. Then, the governing equation for the kth moment is expressed as

$$\frac{\partial m_k(\{x_i\},t)}{\partial t}+\frac{\partial\left(u_j+(u_{th})_j\right)m_k(\{x_j\},t)}{\partial x_j}=\frac{\partial}{\partial x_j}\left(\Gamma\frac{\partial m_k(\{x_j\},t)}{\partial x_j}\right)+kB_1\hbar m_{k-\frac{1}{3}}(\{x_i\},t)\frac{1}{\alpha}+J(v^*)(\{x_i\},t)v^{*k}+\left[\frac{\partial m_k(\{x_i\},t)}{\partial t}\right]_{\text{coag}}(k=0,\ 1,\ 2), \tag{31}$$

where $\frac{1}{\alpha}=\frac{xv_a+(1-x)v_w}{xv_a}$, $\left[\frac{\partial m_k(\{x_i\},t)}{\partial t}\right]_{\text{coag}}$ is calculated using the harmonic mean of the two regimes, namely Equation 20 of the TEMOM-log MOM (I) model in the free molecular regime and TEMOM's model in the continuum regime, to obtain a solution over the entire size regime, which has been verified a reliable scheme for solving SCE (Otto et al., 1999). For the unresolved moment, $m_{k-1/3}$, in Equation 31, the closure model in Equation 19 needs to be used to achieve the final closure of equations. In the implementation of the TEMOM-log MOM (I) model, only the first three order moments need to be explicitly solved.

Many studies have indicated that sulfuric acid tends to gather water molecules to form hydrates. These hydrates are considered to stabilize the vapor and reduce the nucleation rate by a factor of 10^3–10^8 (Vehkamaki et al., 2003). In the present study, the advanced parameterization model of Vehkamaki et al. (2003) is used, which accounts for high-temperature emissions and has been verified to be suitable for the study of particulate matter emitted from engines (Yu et al., 2009). In this new model, the key variables, such as nucleation rate $J(v^*)$, mole fraction, and the total number of molecules of sulfuric acid in a critical cluster are taken as functions of temperature, relative humidity, and total gas-phase concentration of sulfuric acid.

In the model proposed by Vehkamaki et al. (2003), the mole fraction of sulfuric acid x^* in a critical cluster is given by

$$\begin{aligned}x^*=&\,0.847012-0.0029656T-0.00662266\ln(Na)+0.0000587835T\ln(Na)\\&+0.0592653\ln(RH)-0.000363192T\ln(RH)+0.0230074(\ln(RH))^2\\&+0.0000851374T(\ln(RH))^2+0.00217417(\ln(RH))^2\\&-7.923\times10^{-6}T(\ln(RH))^3,\end{aligned} \tag{32}$$

where Na is the total gas-phase concentration of sulfuric acid, T is the absolute temperature, and RH is the relative humidity in percentage form. The nucleation rate is given by an exponential of a third-order polynomial of $\ln(RH)$ and $\ln(Na)$,

$$\begin{aligned}J(v^*)=\exp[&a(T,x^*)+b(T,x^*)\ln(RH)+c(T,x^*)(\ln(RH))^2+d(T,x^*)(\ln(RH))^3+e(T,x^*)\ln(Na)\\&+f(T,x^*)\ln(RH)\ln(Na)+g(T,x^*)(\ln(RH))^2\ln(Na)+h(T,x^*)(\ln(Na))^2\\&+i(T,x^*)\ln(RH)(\ln(Na))^2+j(T,x^*)(\ln(Na))^3,\end{aligned} \tag{33}$$

where the coefficients $a(T,x^*)$ ... $j(T,x^*)$ are functions of temperature T and critical cluster mole fraction x^*. The total number of molecules in the critical cluster N^*_{tot} is given by

$$\begin{aligned}N^*_{tot}=\exp[&A(T,x^*)+B(T,x^*)\ln(RH)+C(T,x^*)(\ln(RH))^2+D(T,x^*)(\ln(RH))^3\\&+E(T,x^*)\ln(Na)+F(T,x^*)\ln(RH)\ln(Na)+G(T,x^*)(\ln(RH))^2\ln(Na)\\&+H(T,x^*)(\ln(Na))^2+I(T,x^*)\ln(RH)(\ln(Na))^2+J(T,x^*)(\ln(Na))^3,\end{aligned} \tag{34}$$

where the coefficients $A(T,x^*)$... $J(T,x^*)$ are also functions of temperature T and critical cluster mole fraction x^*. Detailed definitions of these coefficients can be found in Vehkamaki et al. (2003).

21698996, 2020, 13, Downloaded from https://agupubs.onlinelibrary.wiley.com/doi/10.1029/2019JD032172 by Hong Kong Poly University, Wiley Online Library on [16/05/2024]. See the Terms and Conditions (https://onlinelibrary.wiley.com/terms-and-conditions) on Wiley Online Library for rules of use; OA articles are governed by the applicable Creative Commons License

In addition, several key functions or parameters, including the velocity of thermophoresis, u_{th}, subgrid-scale turbulent diffusivity coefficient, Γ_t, Brownian diffusion coefficient, Γ_b, and the growth rate of particle size due to the arrival and loss of sulfuric acid (H_2SO_4) molecules to the entire droplet surface, G, can be found in Liu, Chan, & Liu (2019).

4.3.1.3. Governing Equations for Gas Species

During numerical simulation, the evolution of gas species, including sulfuric acid and water vapors, must be determined before calculating the moment ODEs. Based on the moment transformation in Equation 4, the differential equations for the evolution of gas species, including sulfuric acid, Y_1, water vapors, Y_2, and CO_2 tracer, Y_3 are expressed as follows:

$$\frac{\partial Y_1}{\partial t}+\frac{\partial u_j Y_1}{\partial x_j}=\frac{\partial}{\partial x_j}\left(D_1\frac{\partial Y_1}{\partial x_j}\right)+R-J\left(v^*\right)k^*-\frac{B_1}{v^*}\hbar m_{2/3}, \tag{35a}$$

$$\frac{\partial Y_2}{\partial t}+\frac{\partial u_j Y_2}{\partial x_j}=\frac{\partial}{\partial x_j}\left(D_2\frac{\partial Y_2}{\partial x_j}\right), \tag{35b}$$

$$\frac{\partial Y_3}{\partial t}+\frac{\partial u_j Y_3}{\partial x_j}=\frac{\partial}{\partial x_j}\left(D_3\frac{\partial Y_3}{\partial x_j}\right), \tag{35c}$$

where k^* is the number of sulfuric acid molecules in the critical cluster denoted by $k^*=N^*_{tot}\cdot x^*$, and R is the birth rate. D_1, D_2, and D_3 are molecular diffusion coefficients of sulfuric acid, water vapors, and CO_2 tracer, respectively. The parameter k^* is obtained from the nucleation model of Vehkamaki et al. (2003).

4.3.2. Configuration of Computational Domain

Figure 5 shows the Cartesian coordinate system (x, y, z) used in the numerical simulations for the vehicle exhaust plume, which is consistent with the experimental setup shown in Ning et al. (2005) and the same as the numerical calculation shown in Yu et al. (2009). The diameter of the vehicle tailpipe is $D = 0.03$ m. The computational domain is 1,000D in x coordinate×333D in y coordinate. In order to make a comparison with the experimental data and the previous numerical calculation data using the TEMOM model, the tailpipe exit velocity used was 4.8 m/s and the exhaust temperature used was 400 K; H_2O and CO_2 account for 6% and 12% in mole fraction, respectively. The velocity of the surrounding air is taken as 0 m/s for the present numerical simulation. The numerical calculation is simplified to be a two-dimensional axisymmetric model in which the vehicle tailpipe is a circular pipe.

All governing equations are discretized using the finite-volume method. The Quadratic Upwind Interpolation for Convective Kinematics scheme is adopted for the convective terms in Equations 28a, 28b, 28c, 30, and 34. For the governing equations accounting for particles and gas species in Equations 30 and 34, user-defined functions in ANSYS Fluent software were utilized. The TEMOM-log MOM (I) in Equation 20 was utilized to calculate the evolution of nanoparticle dynamics due to Brownian coagulation. The calculation time step, t, was fixed at 0.001 s for all numerical simulations for both numerical efficiency and accuracy. In the numerical simulation, all calculations were implemented using normalized parameters; the details for the normalization are the same as in our previous work (Liu, Chan, Lin, et al., 2019; Yu et al., 2009).

4.3.3. Results and Discussions for the Application of the TEMOM-Log MOM (I)

Figure 6 shows the distribution of (a) the velocity magnitude, (b) normalized secondary particle number concentration, (c) normalized particle volume concentration, and (d) nucleation rate of secondary particles. It should be noted that both M_0 and M_1 shown in Figures 6b and 6c are normalized values according to the normalized equation presented in Equation 23. In the turbulent jet flow, the evolution of the large vortex is found to dominate the distribution and evolution of particle quantities, including the particle number concentration, particle volume concentration, average particle size, and geometric standard deviation of particle number distribution in the surrounding air condition (Garrick & Khakpour, 2004; Lin et al., 2016).

The effect of the large vortex on the distribution of statistical moment quantities are represented in Figures 6b and 6c, where the maximum value of particle number concentration appears at the near

21698996, 2020, 13, Downloaded from https://agupubs.onlinelibrary.wiley.com/doi/10.1029/2019JD032172 by Hong Kong Poly University, Wiley Online Library on [16/05/2024]. See the Terms and Conditions (https://onlinelibrary.wiley.com/terms-and-conditions) on Wiley Online Library for rules of use; OA articles are governed by the applicable Creative Commons License

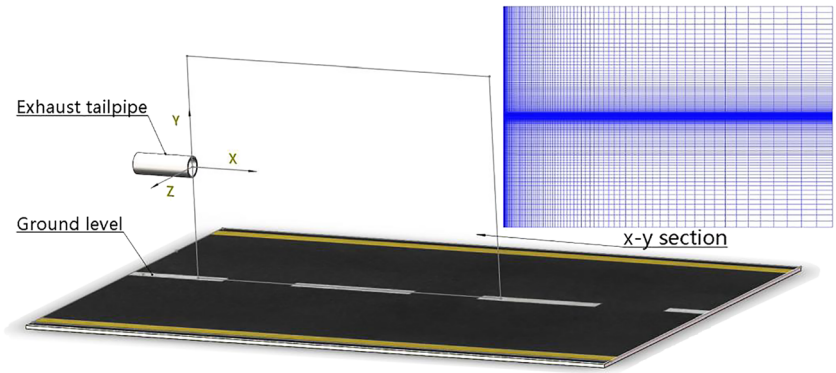

Figure 5. Cartesian coordinate system (*x, y, z*) of the computational domain.

tailpipe exit $x \approx 0.25$–0.35 m due to the strong mixture that occurs between the exhaust jet flow and the surrounding cold air. In the jet region, the exhaust jet plume temperature decreases to a lower level due to mixing with the surrounding cold air, causing binary homogeneous nucleation to occur. It also leads to a high nucleation rate of H_2SO_4-H_2O monomers to occur there, resulting in the high particle number concentration as shown in Figure 6b. However, it is not surprising to observe that the main nucleation rate appears only at the near tailpipe exit region, as shown in Figure 6d, especially as the region is much closer to the tailpipe exit than the high particle number concentration region shown in Figure 6b. Further downstream of the exhaust jet flow, eddies form and entrain the surrounding cold air into the main exhaust jet flow, which decreases the gas temperature in the mixing region but no high particle number concentration is formed.

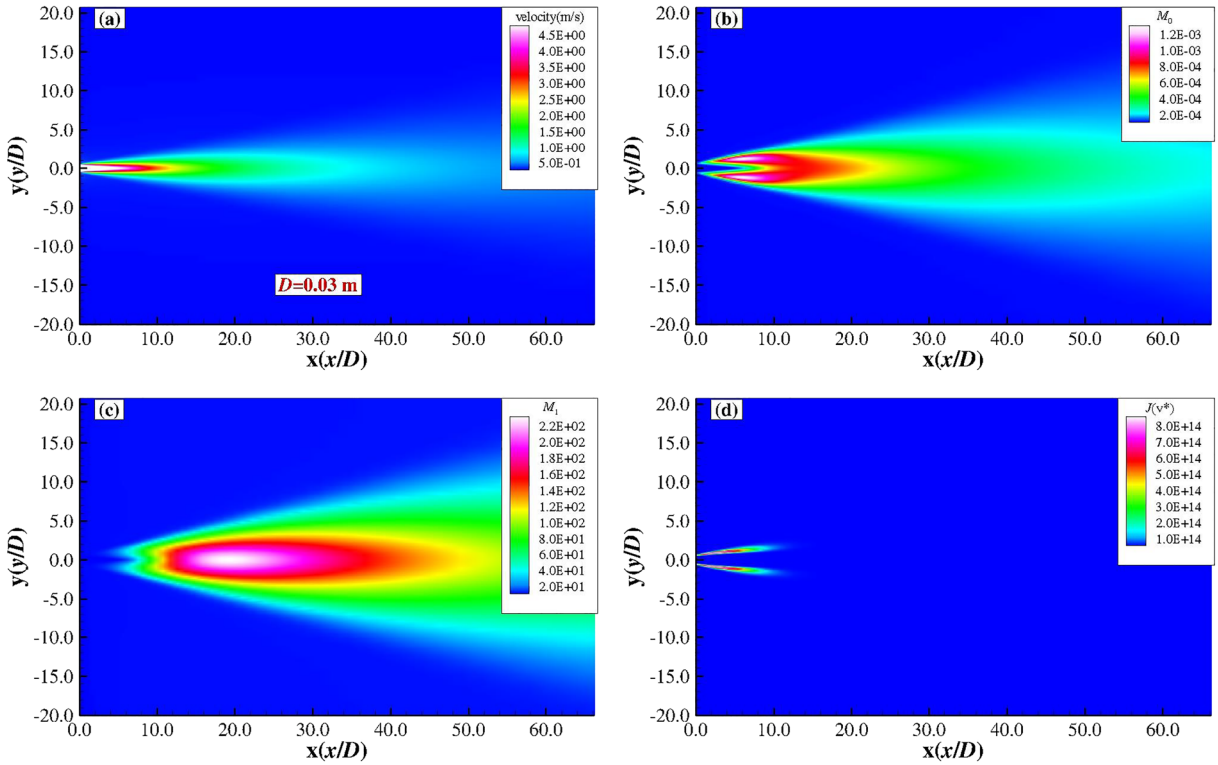

Figure 6. Contours of (a) velocity magnitude (m/s), (b) normalized secondary particle number concentration, M_0, (c) normalized particle volume concentration, M_1, and (d) nucleation rate of secondary particles, $J(v^*)$ (#/(s·m^3).

21698996, 2020, 13, Downloaded from https://agupubs.onlinelibrary.wiley.com/doi/10.1029/2019JD032172 by Hong Kong Poly University, Wiley Online Library on [16/05/2024]. See the Terms and Conditions (https://onlinelibrary.wiley.com/terms-and-conditions) on Wiley Online Library for rules of use; OA articles are governed by the applicable Creative Commons License

In Figure 6c, it can be observed that the particle mass concentration reaches the maximum value away from the tailpipe exit at $x \approx 0.50$–0.70 m. Contrary to the particle number distribution and nucleation rate, particle mass distribution mainly distributes in the centerline of the exhaust jet flow rather than at the jet interface. The evolution and distribution of particle dynamics obtained in this study is consistent with the results obtained from the transient method, such as large eddy simulation (Yu et al., 2009). This is the result of external effects such as convection, diffusion and thermophoresis, and internal dynamic processes (i.e., nucleation, condensation, and coagulation). In Garrick's research team on nanoparticle-laden jet and boundary flows (Garrick, 2011; Miller & Garrick, 2004; Murfield & Garrick, 2013), the new formation of particles on *the turbulent interface* in *boundary* layers is also observed, which is considered to be the main source of particle formation in a turbulent flow.

The radial distance of normalized M_0 and M_1 and nucleation rate at different axial exhaust jet distances, and streamwise distance of particle mean diameter d_p, from the tailpipe exit are shown in Figure 7. Both the newly proposed TEMOM-log MOM (I) model and the widely recognized log MOM model are implemented for comparative study. There are no obvious differences in the four physical quantities investigated of the two MOMs. It should be noted that the log MOM is still the most widely used method in atmospheric aerosol dynamics due to its high numerical efficiency, for example, WRF-Chem in the field of earth science. In Figures 7a and 7b, it is clear that in the region very close to the tailpipe exit, that is, $x = 0.1$ m, the values of both M_0 and M_1 reach their maximum at the region away from the centerline of the exhaust jet flow. Further downstream of the exhaust jet flow where $x = 0.5$ to 2.0 m, the values of both M_0 and M_1 in the centerline region are larger than that in the surrounding region. This implies that in the downstream region, the surrounding air is entrained by large vortices into the nanoparticle-laden multiphase system, which dominates the evolution of particle dynamics rather than the nucleation process. In Figure 7c, the nucleation process only appears at $x = 0.1$ and 0.2 m, while further downstream at $x = 1.0$ m and 2.0 m, no new particle formation takes place. This further supports the conclusion from Figure 6d that the only region in which new particles can be formed is the region very near to the tailpipe exit. In addition, it is clear that the nearer to the tailpipe exit, the higher the rate of nucleation formed. This finding is contrary to the commonly held understanding that new particles are mostly formed in the region where the jet and the surrounding cold air can be strongly mixed in the downstream exhaust jet flow region (Lin et al., 2016). In the present study, only new particle formation is observed in the jet flow boundary, which is very close to the tailpipe exit, while in the downstream exhaust jet flow region where the strong mixture is achieved, no new particle formation is observed. This should contribute to the understanding that the particle number concentration formed of new particles by the main precursor (i.e., H_2SO_4 vapor) cannot meet the minimum requirement to achieve a thermally stable H_2SO_4-H_2O monomer in the downstream exhaust jet flow. The mean particle diameter along the axis is shown in Figure 7d, which is calculated from the following formula,

$$d_p = \left(\frac{6M_1}{\pi M_0}\right)^{1/3} \times d_{g0}. \tag{36}$$

It is obvious that the mean particle diameter increase from its lowest value to its highest value (~30 nm) within the region very close to the tailpipe exit, that is, $x = 0.1$ m. Further downstream of the exhaust jet flow, the mean particle diameter attains its value, which implies that the particle growth mainly takes place very close to the tailpipe due to the both contributions from coagulation and condensation. The model gives the same results from observations that most particles emitted by engines are in the nanoparticle range (i.e., d_p<50 nm) (Harrison et al., 2018; Kittelson, 1998).

5. Conclusions

In all the current atmospheric aerosol dynamics models, the SCE must be included to describe the growth in size of atmospheric aerosols and cloud droplets due to coagulation. However, the numerical solution to the SCE undergoing Brownian coagulation in the free molecular regime is a direct challenge. In this study, a new mathematical method for solving the SCE undergoing Brownian coagulation in a free molecular regime is proposed and developed. In this method, the concept of well-established

21698996, 2020, 13, Downloaded from https://agupubs.onlinelibrary.wiley.com/doi/10.1029/2019JD032172 by Hong Kong Poly University, Wiley Online Library on [16/05/2024]. See the Terms and Conditions (https://onlinelibrary.wiley.com/terms-and-conditions) on Wiley Online Library for rules of use; OA articles are governed by the applicable Creative Commons License

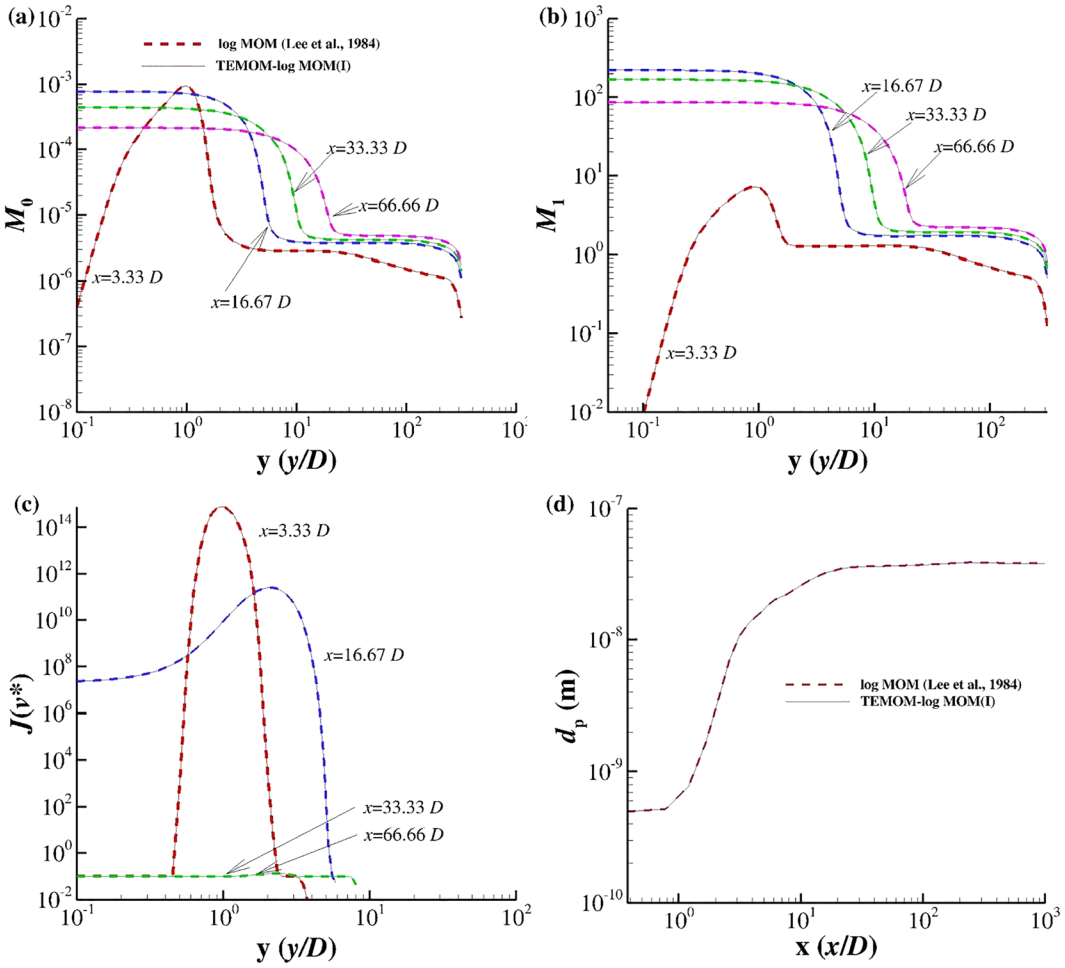

Figure 7. Radial distance y of (a) the normalized secondary particle number concentration, M_0, (b) normalized particle volume concentration, M_1, and (c) nucleation rate of secondary particles at the axial tailpipe exit, x/D = 3.33, 16.67, 33.33, and 66.66. The red dotted line = 3.33, pink dotted line =16.67, green dotted line = 33.33, and blue dotted line = 66.66 in Figures 6a–6c; streamwise distance x of (d) the mean particle diameter, d_p.

TEMOM and log MOM for approximating the collision kernel and implicit moments are hybridized. The numerical precision and efficiency of the new method are evaluated by comparing it to the SM as well as the TEMOM and classic log MOM. The results imply that the new method, in which the collision kernel is approximated with the concept of log MOM and the implicit moments are closed by the concept of TEMOM, has almost the same numerical precision and efficiency as the TEMOM and log MOM. This new method is then successfully applied to the study of secondary nanoparticle formation and subsequent growth of H_2SO_4-H_2O in a turbulent jet plume. With the new method, the formation of new particles only appears in the interface region of the turbulent exhaust jet, which is very close to the tailpipe exit. No new particle was formed in the mixture of the exhaust jet plume and the surrounding cold air downstream. The new method overcomes the limitation of the classical log MOM, that is, that the PSD must follow lognormal particle size distributions with respect to time. Thus, this new method will have wide applications where the atmospheric aerosol size distribution is typically bimodal or multimodal. As one of MOMs, the new method shares a common feature with other MOMs that the computational efficiency is lower than some analytical methods when addressing open systems with large spatial gradients, including the methods presented in Turco and Yu (1997) and Anand and Mayya (2011), due to the additional calculation of Navier-Stokes equations, but it provides higher resolution spatial and temporal maps of aerosols and cloud droplets during dynamic evolution.

21698996, 2020, 13, Downloaded from https://agupubs.onlinelibrary.wiley.com/doi/10.1029/2019JD032172 by Hong Kong Poly University, Wiley Online Library on [16/05/2024]. See the Terms and Conditions (https://onlinelibrary.wiley.com/terms-and-conditions) on Wiley Online Library for rules of use; OA articles are governed by the applicable Creative Commons License

Appendix A

A.1 Derivation of Equation 11

$$\begin{aligned}\beta(v,v_1) &= K(1/v+1/v_1)^{\frac{1}{2}}\left(v^{\frac{1}{3}}+v_1^{\frac{1}{3}}\right)^2 \\ &= K(v+v_1)^{\frac{1}{2}}\left(v^{\frac{1}{6}}v_1^{-\frac{1}{2}}+2v^{-\frac{1}{6}}v_1^{-\frac{1}{6}}+v^{-\frac{1}{2}}v_1^{\frac{1}{6}}\right) \approx Kb_k\left(v^{\frac{1}{2}}+v_1^{\frac{1}{2}}\right)\left(v^{\frac{1}{6}}v_1^{-\frac{1}{2}}+2v^{-\frac{1}{6}}v_1^{-\frac{1}{6}}+v^{-\frac{1}{2}}v_1^{\frac{1}{6}}\right) \\ &= Kb_k\left(v^{\frac{2}{3}}v_1^{-\frac{1}{2}}+2v^{\frac{1}{3}}v_1^{-\frac{1}{6}}+v_1^{\frac{1}{6}}+v^{\frac{1}{6}}+2v^{-\frac{1}{6}}v_1^{\frac{1}{3}}+v^{-\frac{1}{2}}v_1^{\frac{2}{3}}\right) \triangleq \widetilde{\beta}_{\mathrm{Log}}(v,v_1)\end{aligned} \tag{A1}$$

A.2 Derivation of Equation 16

$$\begin{aligned}\beta(v,v_1) &= B_1(1/v+1/v_1)^{\frac{1}{2}}\left(v^{\frac{1}{3}}+v_1^{\frac{1}{3}}\right)^2 \\ &= B_1(v+v_1)^{1/2}\left(v^{1/6}{v_1}^{-1/2}+2v^{-1/6}{v_1}^{-1/6}+v^{-1/2}{v_1}^{1/6}\right) \\ &\approx B_1\left(\frac{3\sqrt{2u}}{8}+\frac{3\sqrt{2}v}{8\sqrt{u}}+\frac{3\sqrt{2}v_1}{8\sqrt{u}}-\frac{\sqrt{2}v^2}{32u^{\frac{3}{2}}}-\frac{\sqrt{2}vv_1}{16u^{\frac{3}{2}}}-\frac{\sqrt{2}v_1^2}{32u^{\frac{3}{2}}}\right)\left(v^{\frac{1}{6}}v_1^{-\frac{1}{2}}+2v^{-\frac{1}{6}}v_1^{-\frac{1}{6}}+v^{-\frac{1}{2}}v_1^{\frac{1}{6}}\right) \\ &= B_1\left[\frac{3}{8}(2u)^{\frac{1}{2}}\left(v^{\frac{1}{6}}v_1^{-\frac{1}{2}}+2v^{-\frac{1}{6}}v_1^{-\frac{1}{6}}+v_1^{\frac{1}{6}}v^{-\frac{1}{2}}\right)+\frac{3}{8}\left(\frac{2}{u}\right)^{\frac{1}{2}}\left(v^{\frac{7}{6}}v_1^{-\frac{1}{2}}+v^{-\frac{1}{2}}v_1^{\frac{7}{6}}+2v^{\frac{5}{6}}v_1^{-\frac{1}{6}}+2v_1^{\frac{5}{6}}v^{-\frac{1}{6}}+v^{\frac{1}{2}}v_1^{\frac{1}{6}}v_1^{\frac{1}{6}}+v^{\frac{1}{6}}v_1^{\frac{1}{2}}\right)\right. \\ &\quad \left.-\frac{1}{32}\left(\frac{2}{u^3}\right)^{\frac{1}{2}}\left(4v^{\frac{5}{6}}v_1^{\frac{5}{6}}+2v^{\frac{7}{6}}v_1^{\frac{1}{2}}+2v^{\frac{1}{2}}v_1^{\frac{7}{6}}+v^{\frac{3}{2}}v_1^{\frac{1}{6}}+v^{\frac{1}{6}}v_1^{\frac{3}{2}}+v^{\frac{13}{6}}v_1^{-\frac{1}{2}}+v^{-\frac{1}{2}}v_1^{\frac{13}{6}}+2v^{\frac{11}{6}}v_1^{-\frac{1}{6}}+2v^{-\frac{1}{6}}v_1^{\frac{11}{6}}\right)\right] \\ &\triangleq \widetilde{\beta}_{\mathrm{Taylor}}(v,v_1).\ \triangleq \widetilde{\beta}_{\mathrm{Taylor}}(v,v_1)\end{aligned} \tag{A2}$$

A.3 Derivation of Equation 23

The kth moment with closure function takes the following expression by assuming the lognormal PSD:

$$\begin{aligned}m_k &= \int_0^\infty e^{ky}\cdot\frac{N_0}{3\sqrt{2\pi}\ln\sigma}e^{-\frac{(y-\ln v_g)^2}{18\ln^2\sigma}}\mathrm{d}y \qquad = \frac{N_0}{3\sqrt{2\pi}\ln\sigma}\int_0^\infty e^{-\frac{y^2-2(\ln v_g+9k\ln^2\sigma)y+\ln^2 v_g}{18\ln^2\sigma}}\mathrm{d}y \\ &= e^{k\ln v_g+\frac{9}{2}k^2\ln^2\sigma}\cdot\frac{N_0}{3\sqrt{2\pi}\ln\sigma}\int_0^\infty e^{-\frac{(y-\ln v_g-9k\ln^2\sigma)^2}{18\ln^2\sigma}}\mathrm{d}y = m_0e^{k\ln(v_g)+\frac{9}{2}k^2\ln^2\sigma},\end{aligned} \tag{A3}$$

where $N_0(=m_0)$ is the initial total number of particles and v_g is the geometric mean volume. Equation A3 can be further expressed in terms of m_0, m_1, and m_2:

$$m_k = m_0^{1-\frac{3}{2}k+\frac{1}{2}k^2}m_1^{2k-k^2}m_2^{-\frac{1}{2}k+\frac{1}{2}k^2}.$$

A.4 Normalized Moment ODEs

When Equation 25 is introduced into Equations 20 and 22, the normalized equations for the hybrid models (I) and (II) are obtained respectively as

21698996, 2020, 13, Downloaded from https://agupubs.onlinelibrary.wiley.com/doi/10.1029/2019JD032172 by Hong Kong Poly University, Wiley Online Library on [16/05/2024]. See the Terms and Conditions (https://onlinelibrary.wiley.com/terms-and-conditions) on Wiley Online Library for rules of use; OA articles are governed by the applicable Creative Commons License

$$
\begin{cases}
\dfrac{\mathrm{d}M_0}{\mathrm{d}\tau} = -\dfrac{\sqrt{2}M_0^{\frac{59}{36}}}{32M_1^{\frac{29}{9}}M_2^{\frac{7}{36}}}\left(\begin{array}{l} -M_0^{\frac{11}{6}}M_1^{\frac{1}{9}}M_2^{\frac{11}{6}} + 12M_0^{\frac{2}{3}}M_1^{\frac{22}{9}}M_2^{\frac{2}{3}} + 11M_0^{\frac{1}{2}}M_1^{\frac{25}{9}}M_2^{\frac{1}{2}} + 12M_0^{\frac{7}{18}}M_1^{3}M_2^{\frac{7}{18}} \\ +24M_0^{\frac{2}{9}}M_1^{\frac{10}{3}}M_2^{\frac{2}{9}} - 2M_0^{\frac{1}{6}}M_1^{\frac{31}{9}}M_2^{\frac{1}{6}} - 2M_0^{\frac{19}{18}}M_1^{\frac{5}{3}}M_2^{\frac{19}{18}} - 2M_0^{\frac{1}{18}}M_1^{\frac{11}{3}}M_2^{\frac{1}{18}} + 12M_1^{\frac{34}{9}} \end{array}\right) \\
\dfrac{\mathrm{d}M_1}{\mathrm{d}\tau} = 0 \\
\dfrac{\mathrm{d}M_2}{\mathrm{d}\tau} = -\dfrac{\sqrt{2}M_0^{-\frac{25}{36}}}{16M_1^{\frac{41}{9}}M_2^{\frac{5}{36}}}\left(\begin{array}{l} M_0^{\frac{23}{6}}M_1^{\frac{1}{9}}M_2^{\frac{31}{9}} - 24M_0^{\frac{11}{9}}M_1^{\frac{16}{3}}M_2^{\frac{5}{6}} - 12M_0^{\frac{5}{3}}M_1^{\frac{40}{9}}M_2^{\frac{23}{18}} + 2M_0^{\frac{13}{6}}M_1^{\frac{31}{9}}M_2^{\frac{16}{9}} + 2M_0^{\frac{55}{18}}M_1^{\frac{5}{3}}M_2^{\frac{8}{3}} \\ +2M_0^{\frac{37}{18}}M_1^{\frac{11}{3}}M_2^{\frac{5}{3}} + M_0^{\frac{5}{2}}M_1^{\frac{25}{9}}M_2^{\frac{19}{9}} - 12M_0^{\frac{1}{2}}M_1^{\frac{61}{9}}M_2^{\frac{1}{9}} - 12M_0M_1^{\frac{52}{9}}M_2^{\frac{11}{18}} - 12M_0^{\frac{7}{18}}M_1^{7} \end{array}\right)
\end{cases}
\tag{A4}
$$

and

$$
\begin{cases}
\dfrac{\mathrm{d}M_0}{\mathrm{d}\tau} = b\dfrac{M_0^{11/6}\left(41M_0^2M_2^2 - 190M_0M_1^2M_2 - 2443M_1^4\right)}{648M_1^{23/6}} \\
\dfrac{\mathrm{d}M_1}{\mathrm{d}\tau} = 0 \\
\dfrac{\mathrm{d}M_2}{\mathrm{d}\tau} = -b\dfrac{65M_0^2M_2^2 - 670M_0M_1^2M_2 - 1987M_1^4}{324M_0^{1/6}M_2^{11/6}}.
\end{cases}
\tag{A5}
$$

Acknowledgments

The authors thank the Zhejiang Provincial Natural Science Foundation of China (LR16A020002) and the National Natural Science Foundation of China (11872353 and 91852102) for their support. In addition, the original files for Figures 2 to 4 and C programs for the hybrid TEMOM-log MOM method have been archived in the Mendeley data at this site (https://doi.org/10.17632/77nrydkfm3.3).

References

Ackermann, I. J., Hass, H., Memmesheimer, M., Ebel, A., Binkowski, F. S., & Shankar, U. (1998). Modal aerosol dynamics model for Europe development and first applications. *Atmospheric Environment*, *32*(17), 2981–2999. https://doi.org/10.1016/S1352-2310(98)00006-5

Anand, S., & Mayya, Y. S. (2011). A simplified approach for solving coagulation-diffusion equation to estimate atmospheric background particle number loading factors contributed by emissions from localized sources. *Atmospheric Environment*, *45*(26), 4488–4496. https://doi.org/10.1016/j.atmosenv.2011.05.016

Anand, S., Mayya, Y. S., Yu, M., Seipenbusch, M., & Kasper, G. (2012). A numerical study of coagulation of nanoparticle aerosols injected continuously into a large, well stirred chamber. *Journal of Aerosol Science*, *52*, 18–32. https://doi.org/10.1016/j.jaerosci.2012.04.010

Barrett, J. C., & Jheeta, J. S. (1996). Improving the accuracy of the moments method for solving the aerosol general dynamic equation. *Journal of Aerosol Science*, *27*(8), 1135–1142. https://doi.org/10.1016/0021-8502(96)00059-6

Bruns, M. C., & Ezekoye, O. A. (2012). Development of a hybrid sectional quadrature-based moment method for solving population balance equations. *Journal of Aerosol Science*, *54*, 88–102. https://doi.org/10.1016/j.jaerosci.2012.07.003

Cai, C., Zhang, X., Wang, K., Zhang, Y., Wang, L., Zhang, Q., et al. (2016). Incorporation of new particle formation and early growth treatments into WRF/Chem: Model improvement, evaluation, and impacts of anthropogenic aerosols over East Asia. *Atmospheric Environment*, *124*(August 2016), 262–284. https://doi.org/10.1016/j.atmosenv.2015.05.046

Chan, T. L., Liu, Y. H., & Chan, C. K. (2010). Direct quadrature method of moments for the exhaust particle formation and evolution in the wake of the studied ground vehicle. *Journal of Aerosol Science*, *41*(6), 553–568. https://doi.org/10.1016/j.jaerosci.2010.03.005

Chan, T. L., & Ning, Z. (2005). On-road remote sensing of diesel vehicle emissions measurement and emission factors estimation in Hong Kong. *Atmospheric Environment*, *39*(36), 6843–6856. https://doi.org/10.1016/j.atmosenv.2005.07.048

Chan, T. L., Zhou, K., Lin, J. Z., & Liu, C. H. (2010). Vehicular exhaust gas-to-nanoparticle conversion and concentration distribution in the vehicle wake region. *International Journal of Nonlinear Sciences and Numerical Simulation*, *11*(8), 581–594. https://doi.org/10.1515/ijnsns.2010.11.8.581

Cohen, E. R., & Vaughan, E. U. (1971). Approximate solution of the equations for aerosol agglomeration. *Journal of Colloid and Interface Science*, *35*(4), 612–623. https://doi.org/10.1016/0021-9797(71)90219-0

Debry, E., Sportisse, B., & Jourdain, B. (2003). A stochastic approach for the numerical simulation of the general dynamics equation for aerosols. *Journal of Computational Physics*, *184*(2), 649–669. https://doi.org/10.1016/S0021-9991(02)00041-4

Fox, R. O., Laurent, F., & Massot, M. (2008). Numerical simulation of spray coalescence in an Eulerian framework: Direct quadrature method of moments and multi-fluid method. *Journal of Computational Physics*, *227*(6), 3058–3088. https://doi.org/10.1016/j.jcp.2007.10.028

Friedlander, S. K. (2000). Smoke, dust and haze: Fundamentals of aerosol behavior. In G. L. Rogers (Ed.), *New York Wiley Interscience* (Chap. 7, 2nd ed.). New York, NY: John Wiley & Sons, Inc.

Gama, C., Ribeiro, I., Lange, A. C., Vogel, A., Ascenso, A., Seixas, V., et al. (2019). Performance assessment of CHIMERE and EURAD-IM' dust modules. *Atmospheric Pollution Research*, *10*(4), 1336–1346. https://doi.org/10.1016/j.apr.2019.03.005

Garrick, S. C. (2011). Effects of turbulent fluctuations on nanoparticle coagulation in shear flows. *Aerosol Science and Technology*, *45*(10), 1272–1285. https://doi.org/10.1080/02786826.2011.589482

Garrick, S. C., & Khakpour, M. (2004). The effects of differential diffusion on nanoparticle coagulation in temporal mixing layers. *Aerosol Science and Technology*, *38*(8), 851–860. https://doi.org/10.1080/027868290503091

Gelbard, F., Tambour, Y., & Seinfeld, J. H. (1980). Sectional representations for simulating aerosol dynamics. *Journal of Colloid and Interface Science*, *76*(2), 541–556. https://doi.org/10.1016/0021-9797(80)90394-X

21698996, 2020, 13, Downloaded from https://agupubs.onlinelibrary.wiley.com/doi/10.1029/2019JD032172 by Hong Kong Poly University, Wiley Online Library on [16/05/2024]. See the Terms and Conditions (https://onlinelibrary.wiley.com/terms-and-conditions) on Wiley Online Library for rules of use; OA articles are governed by the applicable Creative Commons License

Gnach, A., Lipinski, T., Bednarkiewicz, A., Rybka, J., & Capobianco, J. A. (2015). Upconverting nanoparticles: Assessing the toxicity. *Chemical Society Reviews*, *44*(6), 1561–1584. https://doi.org/10.1039/C4CS00177J

Grabowski, W. W., Morrison, H., Shima, S. I., Abade, G. C., Dziekan, P., & Pawlowska, H. (2019). Modeling of cloud microphysics: Can we do better? *Bulletin of the American Meteorological Society*, *100*(4), 655–672. https://doi.org/10.1175/BAMS-D-18-0005.1

Harrison, R. M., Rob Mackenzie, A., Xu, H., Alam, M. S., Nikolova, I., Zhong, J., et al. (2018). Diesel exhaust nanoparticles and their behaviour in the atmosphere. *Proceedings of the Royal Society A: Mathematical, Physical and Engineering Sciences*, *474*(2220), 20180492. https://doi.org/10.1098/rspa.2018.0492

Hass, H., van Loon, M., Kessler, C., Stern, R., Matthijsen, J., Sauter F., et al. (2003). Aerosol modeling: Results and intercomparison from European regional-scale modeling systems. In *A contribution to the EUROTRAC-2 subproject GLOREAM*, 2(January).

Herranz, L. E., Lebel, L., Mascari, F., & Spengler, C. (2018). Progress in modeling in-containment source term with ASTEC-Na. *Annals of Nuclear Energy*, *112*, 84–93. https://doi.org/10.1016/j.anucene.2017.09.037

Herzog, M., Weisenstein, D. K., & Penner, J. E. (2004). A dynamic aerosol module for global chemical transport models: Model description. *Journal of Geophysical Research*, *109*, D18202. https://doi.org/10.1029/2003JD004405

Heylmun, J. C., Kong, B., Passalacqua, A., & Fox, R. O. (2019). A quadrature-based moment method for polydisperse bubbly flows. *Computer Physics Communications*, *244*, 187–204. https://doi.org/10.1016/j.cpc.2019.06.005

Huang, R. J., Zhang, Y., Bozzetti, C., Ho, K. F., Cao, J. J., Han, Y., et al. (2014). High secondary aerosol contribution to particulate pollution during haze events in China. *Nature*, *514*(7521), 218–222. https://doi.org/10.1038/nature13774

Jasor, M. S. G., Polifke, P. W., & Ph, D. (2005). Multi-scale modelling of the population dynamics of hydrometeors with methods of moments.

Karydis, V. A., Tsimpidi, A. P., & Pandis, S. N. (2007). Evaluation of a three-dimensional chemical transport model (PMCAMx) in the eastern United States for all four seasons. *Journal of Geophysical Research*, *112*, D14211. https://doi.org/10.1029/2006JD007890

Kittelson, D. B. (1998). Engines and nanoparticles: A review. *Journal of Aerosol Science*, *29*(5–6), 575–588. https://doi.org/10.1016/S0021-8502(97)10037-4

Kong, B., & Fox, R. O. (2017). A solution algorithm for fluid–particle flows across all flow regimes. *Journal of Computational Physics*, *344*, 575–594. https://doi.org/10.1016/j.jcp.2017.05.013

Korhonen, H., Lehtinen, K. E. J., & Kulmala, M. (2004). Multicomponent aerosol dynamics model UHMA: Model development and validation. *Atmospheric Chemistry and Physics*, *4*(1), 471–506. https://doi.org/10.5194/acpd-4-471-2004

Kostoglou, M. (2007). Extended cell average technique for the solution of coagulation equation. *Journal of Colloid and Interface Science*, *306*(1), 72–81. https://doi.org/10.1016/j.jcis.2006.10.044

Kraft, M. (2005). Modelling of particulate processes. *Kona: Powder Science and Technology in Japan*, *248*(1-4), 450–454. https://doi.org/10.1016/j.apsusc.2005.03.071

Kruis, F. E., Wei, J., van der Zwaag, T., & Haep, S. (2012). Computational fluid dynamics based stochastic aerosol modeling: Combination of a cell-based weighted random walk method and a constant-number Monte-Carlo method for aerosol dynamics. *Chemical Engineering Science*, *70*, 109–120. https://doi.org/10.1016/j.ces.2011.10.040

Kukkonen, J., Olsson, T., Schultz, D. M., Baklanov, A., Klein, T., Miranda, A. I., et al. (2012). A review of operational, regional-scale, chemical weather forecasting models in Europe. *Atmospheric Chemistry and Physics*, *12*(1), 1–87. https://doi.org/10.5194/acp-12-1-2012

Kumar, P., Morawska, L., Birmili, W., Paasonen, P., Hu, M., Kulmala, M., et al. (2014). Ultrafine particles in cities. *Environment International*, *66*, 1–10. https://doi.org/10.1016/j.envint.2014.01.013

Landgrebe, J. D., & Pratsinis, S. E. (1990). A discrete-sectional model for particulate production by gas-phase chemical reaction and aerosol coagulation in the free-molecular regime. *Journal of Colloid and Interface Science*, *139*(1), 63–86. https://doi.org/10.1016/0021-9797(90)90445-T

Lauer, A., Hendricks, J., Ackermann, I., Schell, B., Hass, H., & Metzger, S. (2005). Simulating aerosol microphysics with the ECHAM/MADE GCM—Part I: Model description and comparison with observations. *Atmospheric Chemistry and Physics Discussions*, *5*(5), 7965–8026. https://doi.org/10.5194/acpd-5-7965-2005

Lee, K. W., Chen, H., & Gieseke, J. A. (1984). Log-normally preserving size distribution for Brownian coagulation in the free-molecule regime. *Aerosol Science and Technology*, *3*(1), 53–62. https://doi.org/10.1080/02786828408958993

Lin, J., Pan, X., Yin, Z., & Ku, X. (2016). Solution of general dynamic equation for nanoparticles in turbulent flow considering fluctuating coagulation. *Applied Mathematics and Mechanics (English Edition)*, *37*(10), 1275–1288. https://doi.org/10.1007/s10483-016-2131-9

Liu, H. M., & Chan, T. L. (2018). Differentially weighted operator splitting Monte Carlo method for simulating complex aerosol dynamic processes. *Particuology*, *36*, 114–126. https://doi.org/10.1016/j.partic.2017.04.002

Liu, S., Chan, T. L., Lin, J., & Yu, M. (2019). Numerical study on fractal-like soot aggregate dynamics of turbulent ethylene-oxygen flame. *Fuel*, *256*(November), 115857. https://doi.org/10.1016/j.fuel.2019.115857

Liu, S., Chan, T. L., & Liu, H. (2019). Numerical simulation of particle formation and evolution in a vehicle exhaust plume using the bimodal Taylor expansion method of moments. *Particuology*, *43*(August 2018), 46–55. https://doi.org/10.1016/j.partic.2018.02.003

Marchisio, D. L., & Fox, R. O. (2005). Solution of population balance equations using the direct quadrature method of moments. *Journal of Aerosol Science*, *36*(1), 43–73. https://doi.org/10.1016/j.jaerosci.2004.07.009

Maurya, R. K., Saxena, M. R., Rai, P., & Bhardwaj, A. (2018). Effect of compression ratio, nozzle opening pressure, engine load, and butanol addition on nanoparticle emissions from a non-road diesel engine. *Environmental Science and Pollution Research*, *25*(15), 14,674–14,689. https://doi.org/10.1007/s11356-018-1644-8

McGraw, R., Leng, L., Zhu, W., Riemer, N., & West, M. (2008). Aerosol dynamics using the quadrature method of moments: Comparing several quadrature schemes with particle-resolved simulation. *Journal of Physics: Conference Series*, *125*, 012020. https://doi.org/10.1088/1742-6596/125/1/012020

McGraw, R. (1997). Description of aerosol dynamics by the quadrature method of moments. *Aerosol Science and Technology*, *27*(2), 255–265. https://doi.org/10.1080/02786829708965471

Menz, W. J., Akroyd, J., & Kraft, M. (2014). Stochastic solution of population balance equations for reactor networks. *Journal of Computational Physics*, *256*, 615–629. https://doi.org/10.1016/j.jcp.2013.09.021

Miller, S. E., & Garrick, S. C. (2004). Nanoparticle coagulation in a planar jet. *Aerosol Science and Technology*, *38*(1), 79–89. https://doi.org/10.1080/02786820490247669

Morgan, N., Wells, C., Goodson, M., Kraft, M., & Wagner, W. (2006). A new numerical approach for the simulation of the growth of inorganic nanoparticles. *Journal of Computational Physics*, *211*(2), 638–658. https://doi.org/10.1016/j.jcp.2005.04.027

Müller, H. (1928). Zur allgemeinen Theorie ser raschen Koagulation. *Fortschrittsberichte {ü}ber Kolloide Und Polymere*, *27*(6), 223–250.

21698996, 2020, 13, Downloaded from https://agupubs.onlinelibrary.wiley.com/doi/10.1029/2019JD032172 by Hong Kong Poly University, Wiley Online Library on [16/05/2024]. See the Terms and Conditions (https://onlinelibrary.wiley.com/terms-and-conditions) on Wiley Online Library for rules of use; OA articles are governed by the applicable Creative Commons License

Murfield, N. J., & Garrick, S. C. (2013). Large eddy simulation and direct numerical simulation of homogeneous nucleation in turbulent wakes. *Journal of Aerosol Science*, *60*, 21–33. https://doi.org/10.1016/j.jaerosci.2013.01.009

Nagpure, A. S., Gurjar, B. R., & Kumar, P. (2011). Impact of altitude on emission rates of ozone precursors from gasoline-driven light-duty commercial vehicles. *Atmospheric Environment*, *45*(7), 1413–1417. https://doi.org/10.1016/j.atmosenv.2010.12.026

Ning, Z., Cheung, C. S., Lu, Y., Liu, M. A., & Hung, W. T. (2005). Experimental and numerical study of the dispersion of motor vehicle pollutants under idle condition. *Atmospheric Environment*, *39*(40), 7880–7893. https://doi.org/10.1016/j.atmosenv.2005.09.020

Olin, M., Alanen, J., Palmroth, M. R. T., Rönkkö, T., & Dal Maso, M. (2019). Inversely modeling homogeneous H_2SO_4-H_2O nucleation rate in exhaust-related conditions. *Atmospheric Chemistry and Physics*, *19*(9), 6367–6388. https://doi.org/10.5194/acp-19-6367-2019

Otto, E., Fissan, H., Park, S., & Lee, K. (1999). Log-normal size distribution theory of Brownian aerosol coagulation for the entire particle size range: Part II—Analytical solution using Dahneke's coagulation kernel. *Journal of Aerosol Science*, *30*(1), 17–34. https://doi.org/10.1016/S0021-8502(98)00038-X

Park, S., Lee, K., Otto, E., & Fissan, H. (1999). Log-normal size distribution theory of Brownian aerosol coagulation for the entire particle size range: Part I—Analytical solution using the harmonic mean coagulation. *Journal of Aerosol Science*, *30*(1), 3–16. https://doi.org/10.1016/S0021-8502(98)00037-8

Passalacqua, A., Laurent, F., Madadi-Kandjani, E., Heylmun, J. C., & Fox, R. O. (2018). An open-source quadrature-based population balance solver for OpenFOAM. *Chemical Engineering Science*, *176*, 306–318. https://doi.org/10.1016/j.ces.2017.10.043

Petitti, M., Vanni, M., Marchisio, D. L., Buffo, A., & Podenzani, F. (2013). Simulation of coalescence, break-up and mass transfer in a gas-liquid stirred tank with CQMOM. *Chemical Engineering Journal*, *228*, 1182–1194. https://doi.org/10.1016/j.cej.2013.05.047

Pratsinis, S. E. (1988). Simultaneous nucleation condensation and coagulation in aerosol reactors. *Journal of Colloid & Interface Science*, *124*(2), 416–427. https://doi.org/10.1016/0021-9797(88)90180-4

Rani, S. L., Dhariwal, R., & Koch, D. L. (2014). A stochastic model for the relative motion of high Stokes number particles in isotropic turbulence. *Journal of Fluid Mechanics*, *756*, 870–902. https://doi.org/10.1017/jfm.2014.461

Rosenfeld, D. (2006). Atmosphere. Aerosols, clouds, and climate. *Science (New York, N.Y.)*, *312*(5778), 1323–1324. https://doi.org/10.1126/science.1128972

Rosenfeld, D., Sherwood, S., Wood, R., & Donner, L. (2014). Climate effects of aerosol-cloud interactions. *Science*, *343*(6169), 379–380. https://doi.org/10.1126/science.1247490

Rosenfeld, D., Zhu, Y., Wang, M., Zheng, Y., Goren, T., & Yu, S. (2019). Aerosol-driven droplet concentrations dominate coverage and water of oceanic low-level clouds. *Science*, *363*(6427), eaav0566. https://doi.org/10.1126/science.aav0566

Sabelfeld, K. (1998). Stochastic models for coagulation of aerosol particles in intermittent turbulent flows. *Mathematics and Computers in Simulation*, *47*(2–5), 85–101. https://doi.org/10.1016/S0378-4754(98)00095-0

Sportisse, B. (2007). A review of current issues in air pollution modeling and simulation. *Computational Geosciences*, *11*(2), 159–181. https://doi.org/10.1007/s10596-006-9036-4

Tang, H., & Lin, J. Z. (2013). Modeling of scattering properties of mineral aerosols using modified beta function. *Journal of Geophysical Research: Atmospheres*, *118*, 5570–5587. https://doi.org/10.1002/jgrd.50343

Turco, R. P., & Yu, F. (1997). Aerosol invariance in expanding coagulating plume. *Geophysical Research Letters*, *24*(10), 1223–1226. https://doi.org/10.1029/97GL01092

Van Dingenen, R., & Raes, F. (1991). Determination of the condensation accommodation coefficient of sulfuric acid on water-sulfuric acid aerosol. *Aerosol Science and Technology*, *15*(2), 93–106. https://doi.org/10.1080/02786829108959516

Vehkamaki, H., Kulmala, M., Lehtinen, K. E. J., & Noppel, M. (2003). Modelling binary homogeneous nucleation of water-sulfuric acid vapours: Parameterisation for high temperature emissions. *Environmental Science and Technology*, *37*(15), 3392–3398. https://doi.org/10.1021/es0263442

Vignati, E., Wilson, J., & Stier, P. (2004). M7: An efficient size-resolved aerosol microphysics module for large-scale aerosol transport models. *Journal of Geophysical Research D: Atmospheres*, *109*, D22202. https://doi.org/10.1029/2003JD004485

Vikas, V., Wang, Z. J., & Fox, R. O. (2013). Realizable high-order finite-volume schemes for quadrature-based moment methods applied to diffusion population balance equations. *Journal of Computational Physics*, *249*, 162–179. https://doi.org/10.1016/j.jcp.2013.05.002

Wang, J. S., Chan, T. L., Cheung, C. S., Leung, C. W., & Hung, W. T. (2006). Three-dimensional pollutant concentration dispersion of a vehicular exhaust plume in the real atmosphere. *Atmospheric Environment*, *40*(3), 484–497. https://doi.org/10.1016/j.atmosenv.2005.09.046

Wang, Y., Wang, Y., Wang, L., Petäjä, T., Zha, Q., Gong, C., et al. (2019). Increased inorganic aerosol fraction contributes to air pollution and haze in China. *Atmospheric Chemistry and Physics*, *19*(9), 5881–5888. https://doi.org/10.5194/acp-19-5881-2019

Whitby, E. R., & McMurry, P. H. (1997). Modal aerosol dynamics modeling. *Aerosol Science and Technology*, *27*(6), 673–688. https://doi.org/10.1080/02786829708965504

Wright, D. L., Kasibhatla, P. S., McGraw, R., & Schwartz, S. E. (2001). Description and evaluation of a six-moment aerosol microphysical module for use in atmospheric chemical. *Journal of Geophysical Research*, *106*(D17), 20,275–20,291. https://doi.org/10.1029/2001JD900098

Yao, L., Garmash, O., Bianchi, F., Zheng, J., Yan, C., Kontkanen, J., et al. (2018). Atmospheric new particle formation from sulfuric acid and amines in a Chinese megacity. *Science*, *361*(6399), 278–281. https://doi.org/10.1126/science.aao4839

Yu, M., & Lin, J. (2017a). Hybrid method of moments with interpolation closure–Taylor-series expansion method of moments scheme for solving the Smoluchowski coagulation equation. *Applied Mathematical Modeling*, *52*, 94–106. https://doi.org/10.1080/02786826.2017.1319566

Yu, M. Z., Lin, J., & Chan, T. (2009). Numerical simulation for nucleated vehicle exhaust particulate matters via the TEMOM/LES method. *Int. J. Mod. Phys. C*, *20*(3), 399–421. Retrieved from http://www.worldscinet.com/abstract?id=pii: S0129183109013753

Yu, M., & Lin, J. (2017b). New scheme for implementing the method of moments with interpolative closure. *Aerosol Science & Technology*, *51*(8), 956–971. https://doi.org/10.1080/02786826.2017.1319566

Yu, M., & Lin, J. (2018). Taylor series expansion scheme applied for solving population balance equation. *Reviews in Chemical Engineering*, *34*(4), 561–594. https://doi.org/10.1515/revce-2016-0061

Yu, M., Lin, J., & Chan, T. (2008). A new moment method for solving the coagulation equation for particles in Brownian motion. *Aerosol Science and Technology*, *42*(9), 705–713. https://doi.org/10.1080/02786820802232972

Yu, M., Liu, Y., Jin, G., & Jin, H. (2016). A new analytical solution for agglomerate growth undergoing Brownian coagulation. *Applied Mathematical Modeling*, *40*(9-10), 5497–5509. https://doi.org/10.1016/j.apm.2016.01.009

Yu, M., Liu, Y., & Koivisto, A. J. (2017). An efficient algorithm scheme for implementing the TEMOM for resolving aerosol dynamics. *Aerosol Science and Engineering*, *1*(3), 119–137.

21698996, 2020, 13, Downloaded from https://agupubs.onlinelibrary.wiley.com/doi/10.1029/2019JD032172 by Hong Kong Poly University, Wiley Online Library on [16/05/2024]. See the Terms and Conditions (https://onlinelibrary.wiley.com/terms-and-conditions) on Wiley Online Library for rules of use; OA articles are governed by the applicable Creative Commons License

Yu, M., Liu, Y., Lin, J., & Seipenbusch, M. (2015). Generalized TEMOM scheme for solving the population balance equation. *Aerosol Science and Technology*, *49*(11), 1021–1036. https://doi.org/10.1080/02786826.2015.1093598

Yuan, Q., Xu, J., Wang, Y., Zhang, X., Pang, Y., Liu, L., et al. (2019). Mixing state and fractal dimension of soot particles at a remote site in the southeastern Tibetan Plateau. *Environmental Science & Technology*, *53*(14), 8227–8234. Research-article. https://doi.org/10.1021/acs.est.9b01917

Zhou, C., Zhang, X., Gong, S., Wang, Y., & Xue, M. (2016). Improving aerosol interaction with clouds and precipitation in a regional chemical weather modeling system. *Atmospheric Chemistry and Physics*, *16*(1), 145–160. https://doi.org/10.5194/acp-16-145-2016

Zhou, K., & Chan, T. L. (2011). Simulation of homogeneous particle nucleation in a free turbulent jet. *Aerosol Science and Technology*, *45*(8), 973–987. https://doi.org/10.1080/02786826.2011.572935

21698996, 2020, 13, Downloaded from https://agupubs.onlinelibrary.wiley.com/doi/10.1029/2019JD032172 by Hong Kong Poly University, Wiley Online Library on [16/05/2024]. See the Terms and Conditions (https://onlinelibrary.wiley.com/terms-and-conditions) on Wiley Online Library for rules of use; OA articles are governed by the applicable Creative Commons License